Fate of CO_2 in tallgrass prairie watershed underlain by merokarst bedrock, Konza Prairie, Kansas, USA

by

Katherine R. Andrews

B.S., University of the Pacific, 2019

A THESIS

submitted in partial fulfillment of the requirements for the degree

MASTER OF SCIENCE

Department of Geology
College of Arts and Sciences

KANSAS STATE UNIVERSITY
Manhattan, Kansas

2021

Approved by:

Major Professor
Dr. Matthew Kirk

Copyright

Abstract

Groundwater is a major sink for carbon dioxide (CO_2) generated in soils. Along groundwater flow, mineral weathering and microbial reactions consume some portion of the CO_2, limiting the amount lost to the atmosphere where the groundwater discharges. To better understand the fate of CO_2 in carbonate terrains, we examined variation in groundwater and surface water chemistry in shallow carbonate aquifers at Konza Prairie, in northeast Kansas, USA.

We collected 29 water samples from 11 wells and two stream sites during baseflow conditions in Konza watershed N04d during fall, 2020. The wells are completed in two thin (< 1 m) Permian carbonate units interbedded with mudstones (merokarst). We chemically characterized the water chemistry using standard techniques and used speciation calculations to assess CO_2 concentrations. We also analyzed water isotopes in all samples to assess recharge timing and concentrations of chlorofluorocarbons (CFC-12, CFC-11, CFC-113) and sulfur hexafluoride (SF_6) in nine samples to better understand groundwater residence time.

Water isotope compositions we measured are consistent with precipitation during May each year and apparent groundwater ages range from 2.33 to 35 years for SF_6 and from 33.67 to 49 years for CFC-12. Despite the relatively short residence times, the groundwater appears to have been largely in equilibrium with the carbonate bedrock. Calcite was only slightly undersaturated in most groundwater samples (avg. log Q/K = -0.05) and concentrations of CO_2 and weathering products did not vary significantly with groundwater age. Using a simple inverse-modeling calculation, we estimate that carbonate weathering consumed roughly 60% of the CO_2 present during recharge. Compared to the groundwater samples, calcite was generally further from equilibrium in the stream water. Saturation index values ranged up to 1.54 on warm sampling days (water T > 20°C) and as low as -0.39 on cold days (T near or below 10°C), reflecting the temperature dependence of CO_2 outgassing and its impact on the pH of stream water. Taken together, our results illustrate the rapid nature of carbonate weathering and the strong dependence of CO_2 outgassing on stream water temperature.

Table of Contents

List of Figures

List of Tables

Chapter 1 - Introduction

Carbonate terrains have the potential to act as a sink for soil CO_2 and thus influence the flux of CO_2 from terrestrial environments to the atmosphere. Weathering in carbonate terrains has previously been assumed to have an insignificant long-term impact on atmospheric CO_2 because, over geological time scales, carbonate weathering is balanced by CO_2 release during carbonate deposition (Winnick and Maher, 2018). However, carbonate minerals weather fairly rapidly (Winnick and Maher, 2018) and have the potential to be a major sink for CO_2 on a century timescale (Gaillardet et al., 1999). Therefore, by learning more about weathering in carbonate terrains, we will be better able to predict changes in CO_2 fluxes from terrestrial environments in response to modern climate change (Gaillardet et al., 2019; Sullivan et al., 2019; Wen et al., 2021).

The partial pressure of CO_2 in soils is generally much higher in soils than the atmosphere as a result of plant respiration and organic matter degradation (Macpherson, 2009). During recharge, soil CO_2 is carried into the groundwater and can be converted to carbonate alkalinity over time by mineral weathering (Fig. 1). Carbonate alkalinity is more easily retained within aqueous systems because it does not form a gas and has the potential to precipitate as a carbonate mineral (Kirk et al., 2013; Zeng and Tice, 2014). Therefore, mineral weathering helps regulate how much CO_2 is emitted from aqueous systems.

Reactions describing weathering of limestone ($CaCO_3$) and dolostone ($CaMg(CO_3)_2$) can be written as follows:

$$CaCO_3 + CO_2 + H_2O \leftrightarrow Ca^{2+} + 2HCO_3^-$$

$$CaMg(CO_3)_2 + 2CO_2 + 2H_2O \leftrightarrow Ca^{2+} + Mg^{2+} + 4HCO_3^-$$

Weathering rates increase with increasing concentrations of CO_2 in recharge water (Covington et al., 2015). Therefore, factors that affect the amount of CO_2 generation in soils, such as temperature, moisture, and water fluxes through soils, can affect weathering rates in the underlying bedrock (Sánchez-Cañete et al., 2018).

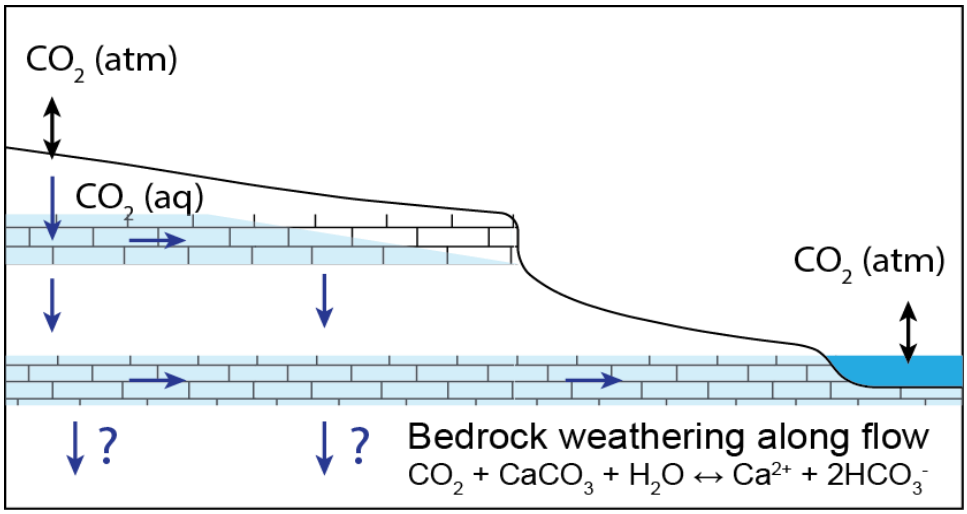

Figure 1. Soil CO_2 is transported to groundwater during recharge and consumed during carbonate bedrock weathering. This prevents some CO_2 from being discharged into the stream water and lost to the atmosphere.

Carbonate environments are widespread and important sources of groundwater. About 25% of Earth's population is partially or completely dependent on karst groundwater aquifers (Hartmann et al., 2014). Therefore, it is important to understand geochemical and hydrologic processes within them, including how they influence the fate of CO_2. Although several previous studies have examined weathering rates in massive carbonates, few have considered rates in carbonate sandwich aquifers (merokarsts). Merokarst environments may differ from massive carbonates because chemical and hydrologic properties of rock layers can vary significantly over short distances.

To learn more about the fate of CO_2 in merokarst terrains, this study considers groundwater residence time and geochemistry in perched aquifers at Konza Prairie. Previous

work by Macpherson and Sullivan (2019) evaluated watershed scale chemical weathering rates from stream water discharge and solute concentration. They found that while there is an increase in chemical weathering rates at the site, decreasing stream discharge has resulted in a reduction of chemical denudation (current rate is 0.02 mm yr^{-1}). However, it remains unclear how chemical weathering may affect the uptake of CO_2 in the subsurface and ultimately, CO_2 loss at the surface water.

For our analysis we examined groundwater flow and concentrations of CO_2 and carbonate weathering biproducts in two shallow carbonate aquifers and the surface water. We sampled 11 wells and 2 stream sites during baseflow conditions to gain insight into the geochemistry at the study site. Water isotopes, dissolved inorganic carbon, and dissolved organic carbon were measured to determine the timing of recharge as well as provide insight into subsurface organic matter degradation. Atmospheric tracers, including chlorofluorocarbons (CFC-12, CFC-11, CFC-113) and sulfur hexafluoride (SF_6), were collected to determine the apparent groundwater ages. Past data was used to assess seasonal trends in CO_2 consumption and loss (Macpherson et al., 2019). Lastly, a CO_2 budget was estimated for the site using our geochemical data and simple mass-balance equations. The results of this study emphasize the rapid nature of chemical weathering within a merokarst environment. Our work highlights the extent to which carbonate weathering can convert CO_2 to alkalinity, preventing loss to the atmosphere that can ultimately impact the century scale global CO_2 budget.

Chapter 2 - Methods

2.1 Study Area

Konza Tallgrass Prairie (Fig. 2) is a long-term ecological research (LTER) site that was established in 1972. Located in northeastern Kansas, it is was once a part of a tallgrass prairie biome, most of which has been converted to cropland, that stretched from southern Canada to Oklahoma (Macpherson et al., 2008). Konza Prairie occupies 35 km^2 and is divided into 60 watersheds (Macpherson et al., 2008).

The N04d watershed (Fig. 2) at Konza Prairie was an ideal location for this research because the site has an extensive record of geochemical data, it contains numerous wells, and the site's land-use history is well known. Previous groundwater geochemical analyses at the watershed span 26.5 years (e.g., Macpherson, 1996; Nippert and Knapp, 2007; Macpherson et al., 2008; Macpherson, 2009; Macpherson and Sullivan, 2019; Sullivan et al., 2019).

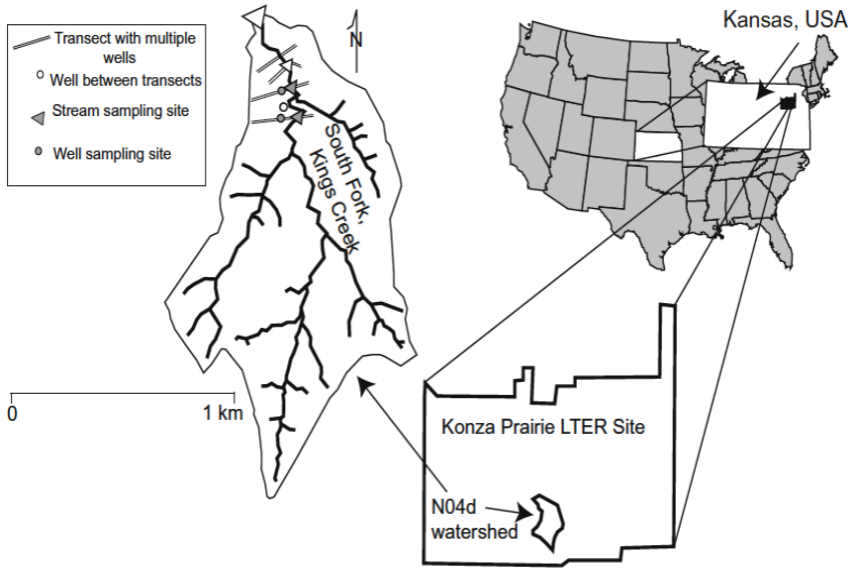

Figure 2. The Konza Prairie LTER site is located in Northeastern Kansas. The watershed that will be the focus of this study, N04d, is drained by Kings Creek south fork. The sampling sites, in this study and the previous study by Macpherson et al. (2008), are located on the lower one-third of the N04d watershed. The wells and sampling sites highlighted in this figure represent all sites sampled in the previous study. Adapted from Macpherson et al., 2008.

Previous data was used to estimate the CO_2 budget at the site as well as the amount of CO_2 consumed in belowground carbonate weathering and the amount of CO_2 potentially lost at surface water sites. Preexisting infrastructure eliminated the need to install wells and set land use control ensured an absence of groundwater contamination from agricultural sources (Tsypin and Macpherson, 2012).

The watershed has a topographic relief of approximately 60 m, a 4-year burn frequency, and grazing by a bison heard that was reintroduced in 1994 (Macpherson et al., 2008). It is characterized by limestone and colluvium-alluvium aquifers. The underlying bedrock is Permian, horizontal, 1-2 m thick, calcite dominant limestone interbedded with 2-4 m thick shale resulting in sandwich-type aquifers (White, 2012). The aquifers are contained in the Beattie Formation, most notably the Morrill limestone and Eiss Limestone (Fig 3). The Morrill limestone is approximately 1.2 m thick. The water table elevation of the aquifer is 6 m and 13 m deep. It is underlain by the Florena Shale and overlain by the Stearns Shale. The Eiss Limestone is a member of the Bader Limestone (Macpherson, 2009). The neo-karst limestone aquifers exhibit solution enlarged joints

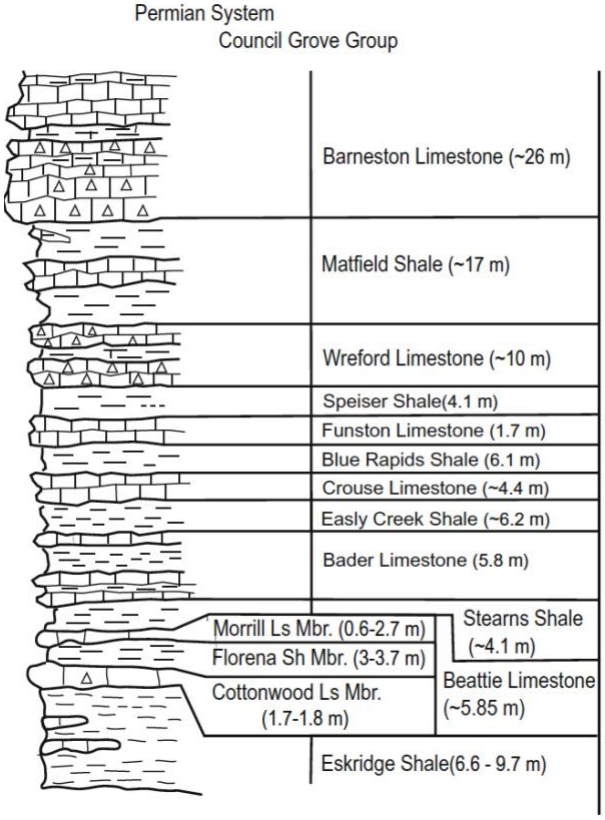

Figure 3. Stratigraphic column shows the Council Grove Group and thickness of each layer listed by the unit name. The Eiss Limestone lies within the Bader Limestone. The Morrill Limestone is within the Beattie Limestone. The two are separated by the relatively thicker Stearns Shale. Adapted from Macpherson et al., 2008.

as secondary porosity (Macpherson et al., 2008). Shallow groundwater chemistry is characteristic of Ca^{2+}, with lesser Mg^{2+}, and HCO_3^- dominated aquifers (Macpherson, 1996). Chemical weathering of carbonates, as typical in a karst environment, play an important role in groundwater pH and alkalinity (Tsypin and Macpherson, 2012).

Communication between the surface water and groundwater is quick, with responses to precipitation resulting in water level and temperature changes within hours (Macpherson, 1996). The groundwater dominated and intermittent Kings Creek empties into McDowell Creek and is a 5^{th} order stream with a drainage area that is entirely within Konza Prairie (Macpherson et al., 2008). Average annual precipitation, concentrated in the spring and early summer, is ~84 cm. Streamflow in the Kings Creek typically stops during the late summer, sometimes continuing to be dry until the fall. The average annual runoff is about 20 cm per year (Mast and Turk, 1999). Monitoring wells have PVC casing that is 5 cm in diameter and a 61 cm PVC slotted well screen at the bottom. They are shielded with a steel well protector and are grouted with bentonite (Macpherson et al., 2008).

2.2 Field Methods

For this study, we collected water samples from 11 wells and two stream sites during baseflow conditions at the watershed in fall, 2020 (Fig. 4). During this study, the 1-1 uptream and 1-1 downstram sites were dry after the first two sampling events and so were only sampled at the beginning of the study. All 36 wells at the N04d watershed were visited in August 2020 for water level measurements. The 11 wells that we sampled were chosen because they were not dry and maintained enough flow to collect samples after purging. 6 of these 11 well sites were sampled every 4-6 weeks to continue a 27 year monitoring effort at the site. During each sampling event, depth to water (DTW) and total depth (TD) were measured using a Solinst water

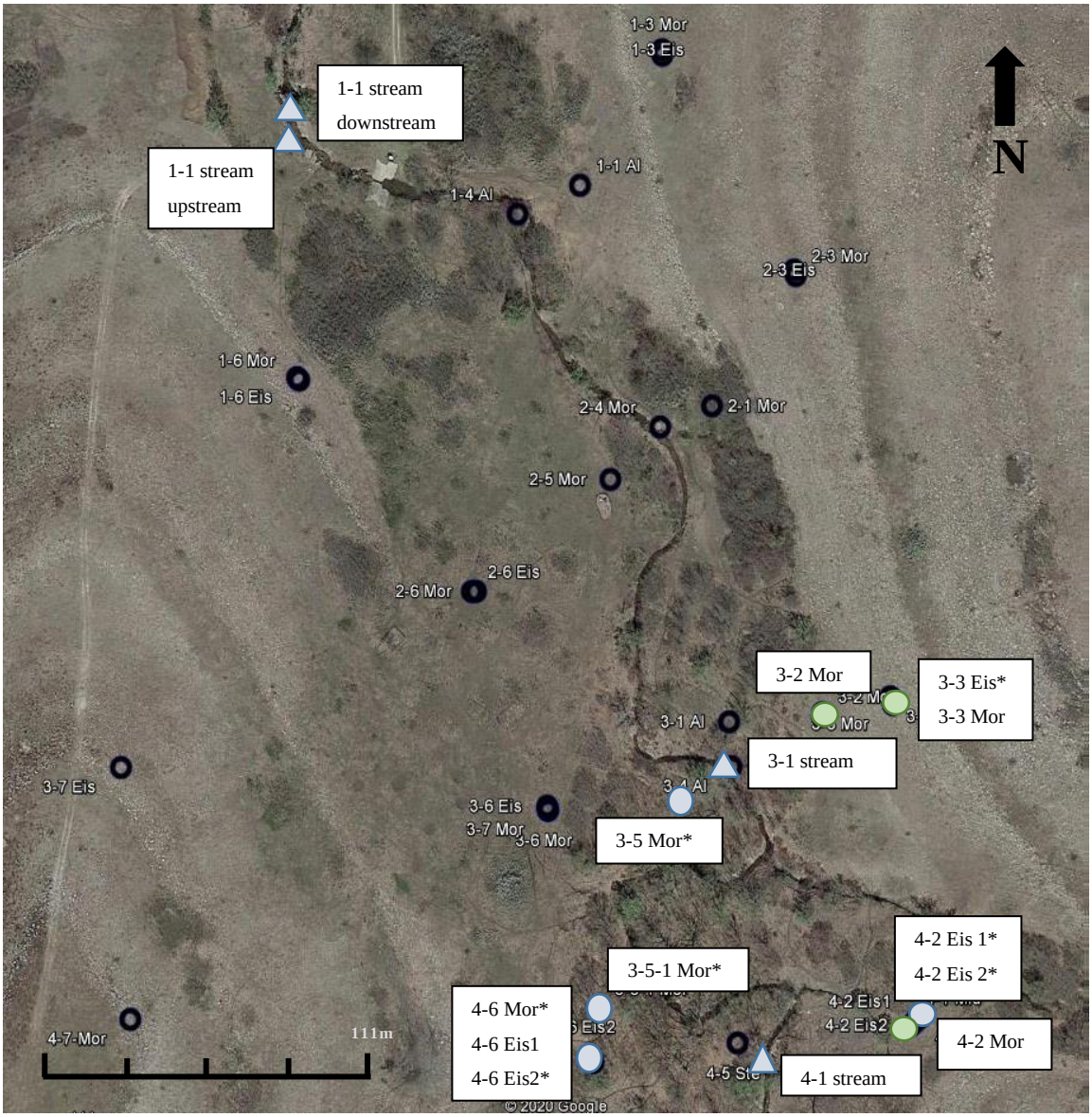

Figure 4. The groundwater (circles) and surface water (triangles) sites that will be the focus of this study are highlighted in blue and green. The black circles represent all 36 well sites in the watershed. The blue color indicates sites that were routinely sampled every 4-6 weeks to continue a 27 year monitoring effort at the site. The green color indicated wells that were sampled once during our study. The 11 wells sampled were chosen based on their ability to maintain enough flow to collect samples after purging. The 1-1 upstream and downstream site was dry for a majority of our study period and was only sampled twice. Asterisks indicate the well was sampled for atmospheric tracers.

level meter. Pressure transducer data was collected if the well was equipped with a Solinst levelogger. Before sampling, the well was purged using a bailer or pump, to remove stagnant water and allow for groundwater that is representative of aquifer to flow into the well. We purged the well until approximately three well volumes were removed. Once purged, we

collected water from a fresh bail and filled a mason jar to measure pH, temperature, conductivity and dissolved oxygen (DO) using a pH and DO probe. For surface water sampling, pH and DO were measured directly from the stream where water was actively flowing.

We sampled major ions and water isotopes to provide insight into the geochemistry of the water as well as recharge timing. These samples were collected by dispensing water through a 60 mL syringe with a filter cartridge and into a 60 mL Nalgene bottle for the major ions and a glass vial for the water isotopes. The cation samples were later acidified with metal grade nitric acid for preservation. All samples were stored in a cooler and refrigerated upon returning to the lab. Dissolved organic carbon samples were analyzed to understand the degree of subsurface organic matter degradation. These samples were collected using a 60 mL syringe with a filter cartridge and were placed into an amber glass bottle and preserved with hydrochloric acid before stored.

Additionally, dissolved inorganic carbon samples were collected to help constrain changes in groundwater chemistry during weathering. Before collecting the water sample, a jar was sterilized with ethanol then filled with the water from the bailer or pump. To preserve the samples for δ^{13}C-DIC analysis, we sterilized the samples by passing them through a 0.22 micron filter and stored them in an autoclaved glass sample vial, sealed with Teflon septum and aluminum crimp seals. A needle was attached to the cartridge and placed into a small serum vile and filled until there was little to no air bubble. The samples were refrigerated and shipped with an ice pack to the lab.

To evaluate groundwater residence time, we collected samples from eight wells for analysis of chlorofluorocarbon (CFC) and sulfur hexafluoride (SF_6) concentrations. We selected wells based on their response to pumping/bailing. We prioritized wells that refilled more quickly during bailing to minimize tracer loss through outgassing. We collected samples using a pump if

the well was able to supply water fast enough to maintain flow during the entire sampling. For those that could not, we used a bailer. To minimize sample disturbance during bailing, we used a bottom emptying device (BED), lowered at slow rate and gently placed into the water to avoid atmospheric contamination. The top 5 cm of water from the bailer were discarded due to possible atmospheric contact. The tube/BED was then placed into the bottom a 500 mL boston round clear glass bottle, which was placed in a two-liter bottle. The bottle and two-liter bottle were allowed to overflow until approximately 2L of water had flown through the tube/BED and out of the bottle. The tube/BED were removed slowly and capped tightly underwater with aluminum lined lids. The bottle was checked for air bubbled and stored upside down until shipment. To assess the consistency of both sampling methods (i.e. the bailer and pump), we sampled two wells with both approaches. CFC-11 and CFC-113 atmospheric concentrations have leveled off and begun decreasing (Walker et al., 2000), so for this study we focused on CFC-12 and SF_6 ages

Depth to water (DTW) as well as total depth (TD) of each well at the field site was measured in Summer 2020. Hydraulic head was calculated by subtracting the depth to water, measured before sampling, from the measuring point elevation. Vertical hydraulic gradients were calculated for nested wells, using the difference in DTW, TD, and well screen midpoints. The potential for downward flow is indicated by positive vertical gradients. A three-point approach was used to determine horizontal hydraulic gradient.

2.3 Geochemical Analysis

Geochemical analyses were carried out in Dr. Kirk's geochemistry lab at the Kansas State University Department of Geology. Major ion (sodium, ammonium, potassium, magnesium, calcite, fluoride, chloride, nitrite, bromide, nitrate, phosphate, and sulfate) concentrations were

analyzed using a Thermo Fisher Scientific ICS-1100 Ion Chromatograph (IC). Detection limits and precision for each ion are provided in Appendix E. Alkalinity was measured using Gran alkalinity titrations with 0.02 N sulfuric acid. Non-purgeable organic carbon (NPOC) was measured using the Shimadzu TOC-L instrument. Water stable isotopes, specifically oxygen ($\delta^{18}O$) and hydrogen (δD) isotopic ratios, were analyzed at 0.1 and 0.5‰ precision, respectively, in the Stable Isotope Mass Spectrometry Laboratory at Kansas State University Division of Biology, using a Picarro L-i2130 water analyzer. Results are expressed in delta notation relative to Vienna Standard Mean Ocean Water (VSMOW). Dissolved inorganic carbon (DIC) $\delta^{13}C$ was analyzed at 0.15‰ precision in the Center for Stable Isotopes at the University of New Mexico using phosphoric acid digestion and a Thermo Delta Plus mass spectrometer with a GasBench system. $\delta^{13}C$-DIC values are expressed in delta notation relative to Vienna Pee Dee Belemnite (VPDB). Atmospheric tracers were sent to be analyzed at the Miami University, Tritium lab by purge-and-trap gas chromatography using electron capture detection. Geochemist's workbench was used to carry out speciation and activity calculations that assessed the favorability of mineral precipitation or dissolution based on how far from equilibrium the water chemistry is with the surrounding bedrock.

Chapter 3 - Results

3.1 Hydrology Results

Hydraulic head ranged from 373.41 to 368.99 meters in the Eiss Limestone and generally decreased N-NW (Appendix B). Below the Eiss, in the Morrill Limestone, hydraulic head ranged from 364.51 to 363.73 meters and generally decreased S-SE, with the exception of flow between 3-5 MOR and 3-5-1 MOR. Between these wells hydraulic head was consistent with flow SW. Using a three-point approach, we estimated horizontal gradients that are consistent with NW flow in the Eiss along a gradient of 0.05 and S-SE flow in the Morrill along a gradient of 0.01. Vertical gradients calculated for nested wells were positive, with an average gradient of 1.20, consistent with downward flow between aquifers.

Our analysis of residence time tracers indicates that groundwater in the carbonate units is relatively young (Appendix D). The average CFC-12 age was 37.5 years and the average SF_6 age was 14 years. Groundwater sampled from the uppermost aquifer in this study, the Eiss Limestone, had younger residence times than water sampled from the Morrill Limestone (Fig. 5). Groundwater from the Eiss Limestone ranged from CFC-12 ages of 38 to 33 years, with an

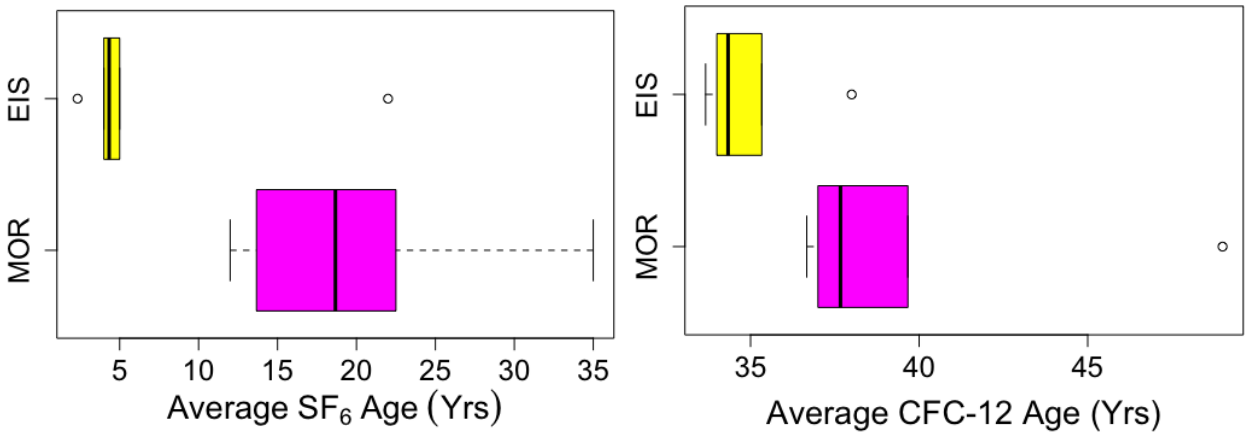

Figure 5. Boxplots of CFC-12 and SF_6 ages in the Eiss and Morrill Limestone aquifers. Groundwater sampled from the Eiss Limestone had younger residence times than that sampled from the Morrill Limestone.

average of 35.10 years, and ranged from SF_6 ages of 25 to 2 years, with an average of 7.53 years. While water from the Morrill Limestone ranged from CFC-12 ages of 49 to 36 years, with an average of 40 years, and ranged from SF_6 ages of 35 to 13 years, with an average of 20.37 years.

The isotopic composition of the groundwater and surface water samples varied little (Appendix C). The oxygen ($\delta^{18}O$) and hydrogen (δD) isotopic ratios of the groundwater and surface water ranged from -3.8 to -4.5 ‰ VSMOW for $\delta^{18}O$ and -27 to -31 ‰ VSMOW for δD. These values were plotted on a local meteoric water line (LMWL), calculated from precipitation water isotope values from the past 20 years at Konza Prairie (personal communication, Dr. Jesse Nippert) (Fig. 6). Using the University of Utah Online Isotopes in Precipitation Calculator, we plotted the average monthly isotopic values from Konza Prairie. A best fit line was added to the data using the equation y = 7.4038x + 2.353, where y is δD and x is $\delta^{18}O$. We then added our measured $\delta^{18}O$ values to the LMWL. These values plotted tightly around May and September precipitation isotope values.

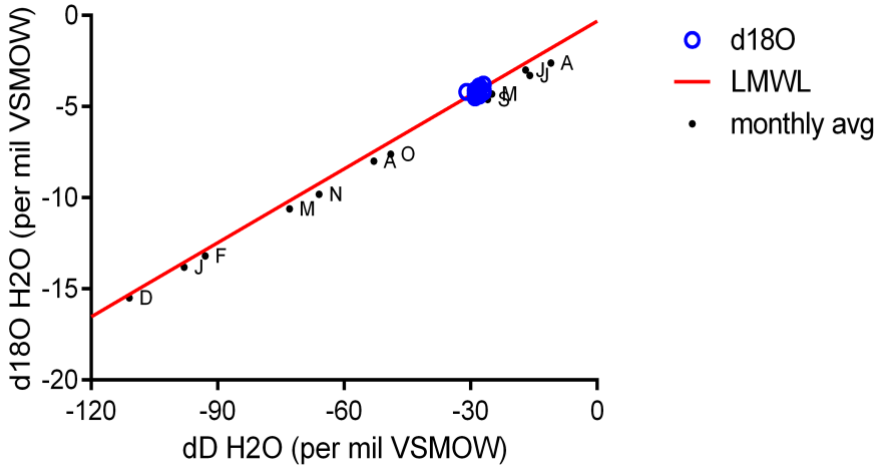

Figure 6. Variation in the oxygen ($\delta^{18}O$) and hydrogen (δD) isotopic ratios of the groundwater and surface water at the study site. These values are plotted along the local meteoric water line (LMWL), shown in red. The LMWL was derived from water isotope values from the past 20 years at Konza Prairie and plotted using the University of Utah Online Isotopes in Precipitation Calculator. A best fit line was fitted to the data (y = 7.4038x + 2.353, where y is (δD and x is $\delta^{18}O$). The δ18O values of our samples are shown as blue circles.

3.2 Water Chemistry

Values of pH, conductivity, and dissolved oxygen (DO) measured in the field were generally higher in the stream than in groundwater samples (Appendix A). Groundwater samples had an average conductivity and pH of 0.57 mS/cm and 6.88, respectively. Both were slightly higher in stream water, averaging 0.611 mS/cm and 7.28, respectively. DO levels in groundwater from the Eiss aquifer ranged from 1.4 to 9.2 mg/L and in the Morrill, it ranged from 1.7 to 10 mg/L. In contrast, dissolved oxygen concentrations in the stream ranged from 8.3 to 10.4 mg/L.

Several ion concentrations, including fluoride and nitrate, as well as alkalinity showed little variation in groundwater and stream samples (Appendix A) (Fig. 7). The average fluoride concentrations in groundwater from the Morrill and Eiss limestones were 0.45 and 0.41 mg/L, respectively. By comparison, fluoride concentrations in stream water samples were only slightly lower, with an average of 0.39 mg/L. Nitrate concentrations in the Morrill had an average of 0.44 mg/L, the Eiss had an average of 0.72 mg/L, and the stream had an average of 0.33 mg/L. In the Morrill, alkalinity had an average of 6.39 meq/L and alkalinity in the Eiss was similar, with an average of 6.63 meq/L. Stream alkalinity was comparable to the groundwater, with an average of 6.19 meq/L.

Two samples within the Morrill limestone had relatively high concentrations of chloride, sodium, and potassium while most other samples showed little variation from the Eiss Limestone and stream water (Appendix A). One of these samples was collected from the 3-3 MOR well, which was only sampled once, and the other was from the 4-6 MOR well. The chloride concentrations in the Morrill were as high as 60.59, with all but the two samples falling between 3.88 to 2.33 mg/L. The groundwater from the Eiss aquifer and stream water had similar chloride concentrations to a majority of the samples from the Morrill. The Eiss had an average chloride

concentration of 3.14 mg/L and the stream had an average of 2.71 mg/L. The same trend was observed in sodium concentrations, with values as high as 16.47 mg/L in the two Morrill samples. Most samples from the Morrill fall between 7.15 to 2.73 mg/L. Similarly, in the Eiss, sodium concentration ranged from 7.22 to 2.34 mg/L while stream concentrations were slightly lower than the groundwater and ranged from 5.28 to 3.69 mg/L. Furthermore, potassium concentrations were as high as 58.63 mg/L in the two samples, however, most potassium concentrations in the Morrill groundwater ranged from 2.51 to 0.76 mg/L, with an average of 1.44 mg/L. In the Eiss, potassium concentrations had an average of 1.74 mg/L. Similar to chloride and sodium, stream concentrations had a lower average of 1.00 mg/L.

Where ion concentrations did differ, they revealed a slight variation in geochemistry between the limestones aquifers and illuminated similarities between groundwater in the Morrill aquifer and the surface water (Appendix A) (Fig 7). For example, in the Morrill, sulfate concentration ranged from 54.43 to 14.25. 4-6MOR and 3-5MOR show an increasing trend in sulfate during the 6-month sample period that may be the result of dissolving gypsum deposits. Stream samples showed a similar increasing trend and had sulfate concentrations ranging from 57.16 to 17.79 mg/L. In contrast, the sulfate concentration within the Eiss did not show this trend and ranged from 38.05 to 7.82 mg/L. To add to this trend, calcium concentrations within the Morrill had an average of 95.80 mg/L and stream water calcium concentrations had an average of 95.72 mg/L. In the Eiss, calcium concentrations were slightly lower and had an average of 91.44 mg/L. Magnesium concentrations were an exception to this trend. In the Morrill, magnesium concentrations ranged from 38.52 to 13.03 mg/L. Magnesium concentrations were slightly lower in the Eiss, varied from 26.03 to 8.69 mg/L. The stream had less variation than the groundwater, with magnesium concentrations that ranged from 21.58 to 17.76 mg/L.

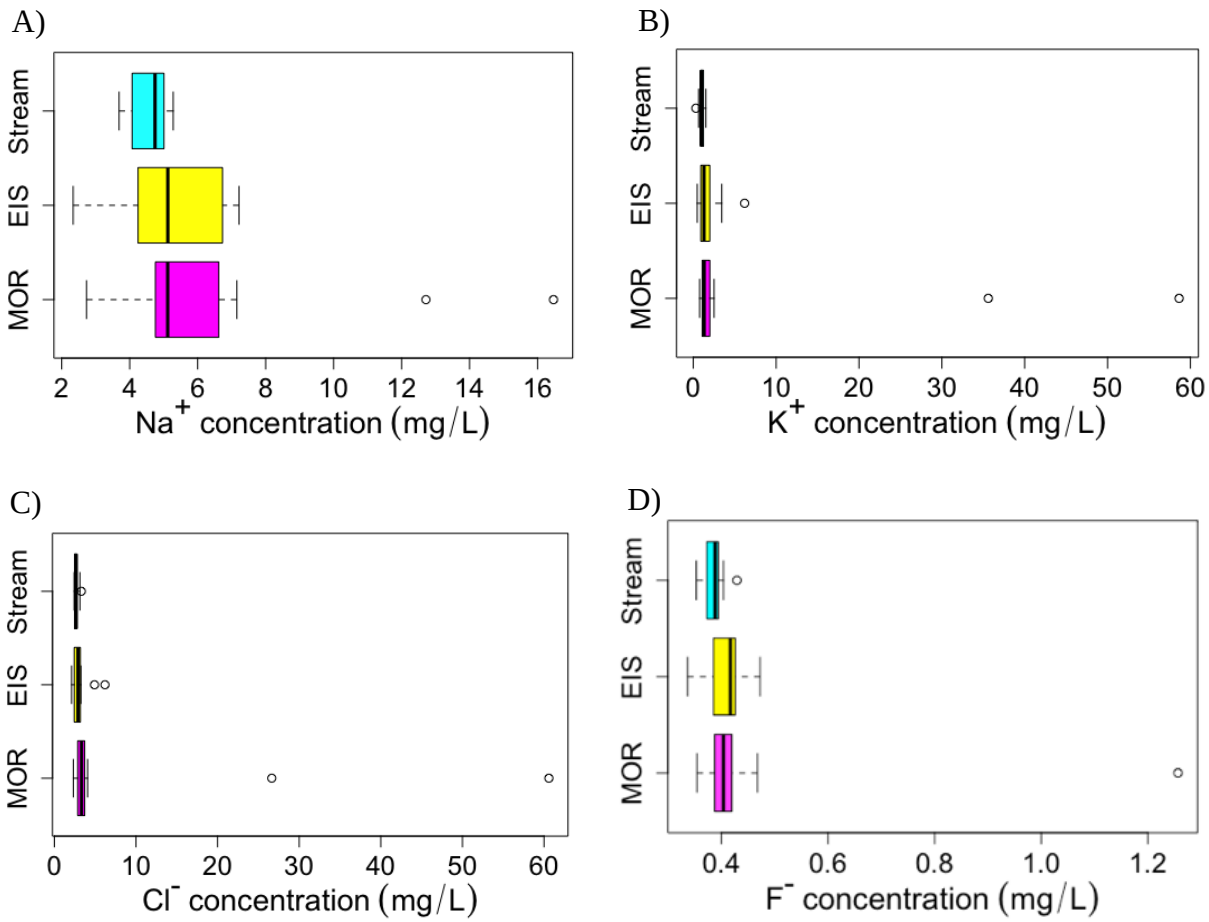
A)
Stream
EIS
MOR
2
4
6
8
10
12
14
16
Na+ concentration (mg/L)
B)
Stream
EIS
MOR
0
10
20
30
40
50
60
K+ concentration (mg/L)
C)
Stream
EIS
MOR
0
10
20
30
40
50
60
Cl- concentration (mg/L)
D)
Stream
EIS
MOR
0.4
0.6
0.8
1.0
1.2
F- concentration (mg/L)

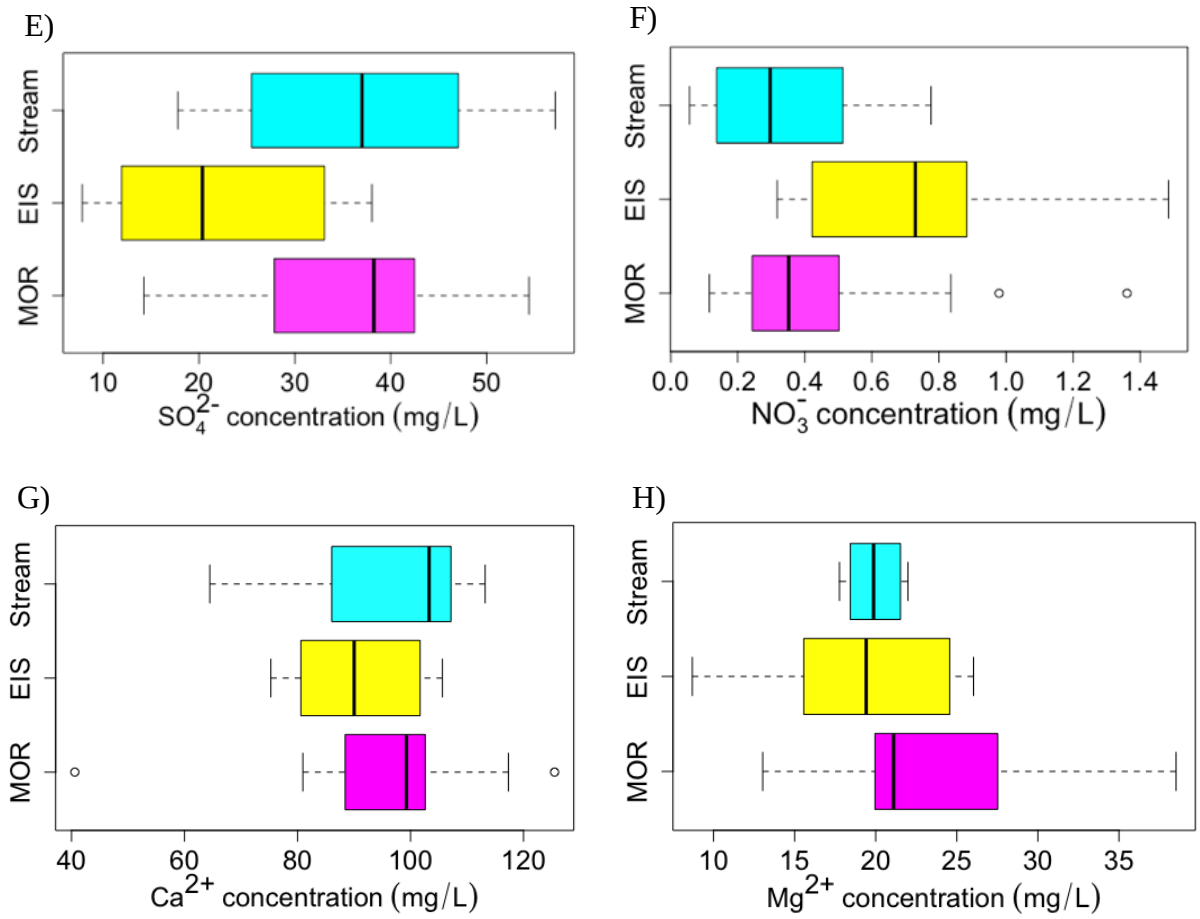

Figure 7. Box plots showing the variation in concentration of (a) sodium, (b) potassium, (c) chloride, (d) fluoride, (e) sulfate, (f) nitrate, (g) calcium, and (h) magnesium in the groundwater sampled from the Morrill limestone and Eiss limestone aquifers as well as the stream water at the study site.

Saturation Indices (SI) indicate whether the water is saturated, undersaturated or oversaturated in respects to certain minerals, thus providing an understanding into the favorability of mineral dissolution or precipitation. Carbonate mineral SI showed little variation in the groundwater compared to surface water (Appendix A). We calculated calcite SI values to be only slightly undersaturated in both units (log Q/K < -0.05). Dolomite was slightly oversaturated in both units. In the Morrill Limestone, the average dolomite SI was 0.39 while in the Eiss Limestone it was 0.32. Compared to the groundwater, the stream was further from

equilibrium, with calcite saturation indices ranging from log Q/K = 1.541 to -0.385 and dolomite SI ranging from log Q/K = 2.541 to -0.456.

NPOC ranged to higher levels in the groundwater than stream samples (Appendix C). In the Eiss Limestone, NPOC values range from 0.70 to 3.18 mg/L. Similarly, in the Morrill Limestone, the NPOC values range from 0.86 to 4.38 mg/L. The groundwater from both aquifers show a decreasing trend in values downgradient. In contrast, the two stream sites NPOC values were 1.16 mg/L at the 4-1 stream site and 1.33 mg/L at the 3-1 stream site.

δ^{13}C-DIC isotopic values were lower in the Morrill Limestone than the Eiss Limestone (Appendix C). In the Eiss Limestone, δ^{13}C-DIC isotopic values ranged from -7.86 to -4.72 ‰ VPDB. In the Morrill Limestone, values were slightly more negative and ranged from -10.04 to -5.07‰ VPDB. Only two samples were collected along the stream. At the furthest upstream site, the isotopic value was -10.04 ‰ VPDB and at a downstream site, the value was -6.79 ‰ VPDB.

Chapter 4 - Discussion

This study seeks to understand how variations in groundwater and surface water geochemistry can help explain the movement of CO_2 through the system. To do so, we assessed the movement of groundwater through the bedrock and considered trends in solute concentrations. We examined differences and similarities between groundwater and surface water chemistry. Lastly, we focused on the fate of CO_2 within the system and the extent to which chemical weathering impacts CO_2 consumption.

4.1 Groundwater Hydrology

Given the lack of rainfall in the region during September, water isotope values are consistent with the predominant recharge period being around May. This supports prior research (Tsypin and Macpherson, 2012) that showed a shift in precipitation patterns, and ultimately recharge patterns, towards an increase in growing season (Apr – Sep) precipitation over time. While groundwater recharge was historically greater in the cold season, several factors suggest an increase in growing season recharge, including a shift to unimodal (June) monthly maximum precipitation, a change in warm to cold season precipitation ratio, and an increase in precipitation during the growing season (Macpherson et al., 2019). Soil CO_2 levels are at a maximum during the summer, when respiration rates are increased in the top of the soil profile, and at a minimum during the winter (Hendry et al., 1999). Increased recharge during warm seasons, therefore, have the potential to increase the annual flux of CO_2 into the subsurface.

Following recharge, our hydraulic head results indicate groundwater flows mostly N-NW in the Eiss Limestone and S-SE in the deeper Morrill Limestone. Flow between the 3-5 MOR and 3-5-1 MOR well appears to be an exception, where hydraulic head is locally consistent with flow southwest. A previous study hypothesized that a collapse feature may be near the 3-5 MOR

and 3-5-1 MOR well (Barry, 2018). Thus, the flow between these two wells is consistent with this possibility. The previous study also included a dye test at the study site that revealed there is likely flow between the aquifers via leaky aquitards (Barry, 2018). This is consistent with our calculated vertical gradient being positive, indicative of the possibility of downward flow between units. However, downward flow throughout the watershed will be dependent on the permeability of the shale layer that lies between the two limestones and the conduit morphology of the limestone units.

Atmospheric tracer analyses provide an understanding into residence times we observe in the groundwater, with an average CFC-12 age of 37.53 yrs. and average. SF_6 age of 13.95 yrs. The differences in ages between the two tracers may be the result of excess air, which describes the air bubbles trapped in water during recharge (Darling et al., 2012). While a standard amount of excess air is assumed to be present in most groundwater samples and is corrected based on the recharge temperature and elevation. It is possible that the excess air present is greater than account for or more variable, which would most effect the SF_6 ages, making them appear relatively younger (Darling et al., 2012). Another factor that can affect the apparent age derived from samples is recharge temperature (Darling et al., 2012). The water isotopic values suggested that we had limited variability in recharge temperature. Therefore, we can assume that the recharge temperature for our samples should not have a significant impact on our apparent age. CFC-12 ages may also be altered when recharge occurs in environments that produce methane, such as wetlands, which is not relevant to our study area (Happell et al., 2003). Furthermore, SF_6 ages can be skewed by igneous or volcanic material, however, none is present at our site (Darling et al., 2012). Overall, SF_6 may be the most reliable tracer for this study because the SF_6 atmospheric concentration continues to rise while CFC-12 atmospheric concentration has begun

to flatten out. Additionally, SF_6 ages are more accurate for water recharged after 1970 (Happell et al., 2003).

Understanding trends in groundwater residence time allows for insight into groundwater movement. We hypothesized that the apparent age of the groundwater would increase as the distance downgradient increased. Using R studio, we identified these trends. Given the small number of samples (n=10), the relationships are not statistically significant ($p < 0.05$) but still provide information on how residence time is influenced by different physical parameters. In the Eiss limestone, the SF_6 and CFC-12 ages increase downgradient. In the Morrill, CFC-12 ages also increase downgradient, however, SF_6 ages show a slightly decreasing trend. This may be the result of a potential collapse feature in the Morrill limestone near the 3-5 MOR and 3-5-1 MOR well that would cause older residence time estimates at these well, which are further up the gradient than the other sites (Barry, 2018). We do observe that the 3-5-1 MOR well has relatively older ages for all atmospheric tracers, with an average age ~10 years greater than the next highest average age.

4.2 Water Chemistry

Dissolved inorganic carbon data provides insight into water movement once it enters the aquifers. As water recharges through soils, which have lighter δ^{13}C-DIC isotopic values, flows through carbonate rock, with heavier δ^{13}C-DIC isotopic values, we would expect the δ^{13}C-DIC value to become less negative downgradient. Opposite of this expected trend, the overall results indicated that water sampled from the Morrill had a lighter signature than water sampled from the Eiss on a watershed-scale. However, when examining results of wells nearby one another or in nests, the δ^{13}C-DIC results are consistent with heavier isotopic values downgradient and in waters with longer residence times. For example, the 3-3 EIS well is downgradient of the 4-2 EIS

1 and 4-2 EIS 2 wells and has a longer residence time. The 4-2 EIS 1 well has a δ^{13}C-DIC value of -7.41 ‰ VPDB and 4-2 EIS 2 has a δ^{13}C-DIC value of -7.77 ‰ VPDB, both are relatively lighter than the 3-3 EIS well, with a δ^{13}C-DIC value of -5.53 ‰ VPDB. This trend is consistent throughout the watershed, with the exception of the 4-6 MOR, 4-6 EIS 1, and 4-6 EIS 2 well nest. At this location, the relatively older 4-6 MOR well has a lighter δ^{13}C-DIC isotopic signature (-9.86 ‰ VPDB) than the younger, overlying 4-6 EIS 1 and 4-6 EIS 2 wells (-6.62 and -5.73 ‰ VPDB, respectively). One possible explanation for this exception is the presence of organic dye in the 4-6 EIS wells, placed there during a previous study (Barry, 2018). Although organic and not analyzed during the δ^{13}C-DIC analysis, this dye may be undergoing degradation and contributing to the DIC pool and thus affecting the isotopic ratio at these wells. In the stream, the isotopic value was -10.04 ‰ VPDB at the upstream site and -6.79 ‰ VPDB at the downstream site. This may reflect CO_2 degassing at the surface water during the day of sampling.

At the study site, we observe that NPOC values decrease downgradient while O_2 persists in the groundwater, suggesting that subsurface organic matter degradation is small relative to organic matter degradation and CO_2 generation in overlying soils. Consistent with this interpretation, O_2 it is available even in groundwater with longer residence times despite relatively lower O_2 concentrations in the groundwater.

We examined spatial trends in solutes and saturation indices to understand how far from equilibrium the water is with the bedrock. We found that although atmospheric tracer data suggesting relatively short residence times, the groundwater is largely in equilibrium with the bedrock. Calcite saturation indices for both units are only slightly undersaturated, with average log Q/K = -0.04. Along groundwater flow path, we would expect increased chemical weathering

product concentrations due to increased water-rock interactions and thus, carbonate bedrock weathering. However, when performing statistical analyses, we observed that mineral weathering product concentrations do not vary significantly with groundwater age and spatial trends in solutes are not significant ($p > 0.05$), further supporting that the groundwater is largely in equilibrium with the bedrock. The outliers in the Morrill samples, including a sample from 4-6 MOR and 3-3 MOR, were possibly contaminated in regard to chloride, sodium, or potassium ions. The 4-6 MOR well was sampled repeatedly and no other samples from this well showed similar spikes in these concentrations. Additionally, past data did not show any trends in increased chloride, sodium, or potassium concentrations from these wells.

Despite conditions in the aquifers, we observe that conditions within the stream are more variable. Along the surface water gradient, there is an decreasing trend in mineral weathering product concentrations that suggest chemical precipitation takes place within the stream. Compared to the groundwater, calcite was further from equilibrium, with calcite saturation indices ranging from log Q/K = 1.541 to -0.385. Furthermore, surface water saturation indices, pH, and dissolved CO_2 concentrations shifted with changes in water temperature. The saturation indices and pH were higher on warm days ($T > 20°C$) and lower on colder days ($T \sim 10°C$ or below). Dissolved CO_2 concentrations showed an opposite trend, with higher concentrations (up to 4.35 mmol) on cold days and lower concentrations on warm days (as low as 0.11 mmol). This variability is driven by changes in CO_2 solubility with temperature, as CO_2 is more soluble under colder conditions, and imply calcite may be dissolving or precipitating in the stream depending on the weather. These trends also reflect the temperature dependency of CO_2 outgassing. This CO_2 loss at the surface water helps explain observed differences between groundwater and surface water pH and saturation indices.

4.3 CO_2 Budget

When mineral dissolution does take place, dissolved CO_2 concentration decreases. By estimating how much CO_2 is taken up by chemical weathering, we can provide insight into the amount of outgassing that could be possible at the surface water. Using mass-balance equations we estimated the CO_2 budget at the N04d watershed (Appendix F).

$$CO_2 \text{ consumed} + CO_2 \text{ present} = CO_2 \text{ inital}$$

CO_2 consumed was approximated by using chemical reaction equations to determine how much CO_2 would be taken up during dolomite dissolution to produce the magnesium concentration present in the water. Then, the remaining calcium, not accounted for by dolomite dissolution, was used to determine how much CO_2 would be consumed during calcite dissolution. Adding these values together gives us the total CO_2 consumed, which when added to the CO_2 concentrations already present in the water provides us with the initial dissolved CO_2 concentration of the groundwater.

For this study, we assume all calcium and magnesium present in the groundwater is derived from carbonate mineral weathering. Uncertainties in this assumption are that some Ca^{2+} and Mg^{2+} is derived from the dissolution of other minerals, such as anhydrites, which are present but not abundant at the site (Gunal and Ransom, 2005; Presley et al., 2010). Another possibility is additional calcite sourced from dry deposition (Simonson, 1995; Mason and Jacobs, 1998). Lastly, it is possible some Ca^{2+} and Mg^{2+} may derive from precipitation (Macpherson and Sullivan, 2019).

Using all groundwater samples that were collected during our study period, we estimated that belowground chemical weathering consumed on average about 60% of the CO_2 that was initially present during recharge (Fig. 8). On average, about 3.3 mmol CO_2 per liter of

groundwater was consumed per day by carbonate weathering during the study. These results highlight the extent to which carbonate weathering in merokarst topography can act as a sink for CO_2 and the rapid nature of chemical weathering in these terrains. More than half of the CO_2 present during recharge is consumed and otherwise prevented from being released to the atmosphere from the surface water. These estimates could change depending on long-term shifts in belowground calcite saturation indices that could drive the system in favor of increased carbonate weathering or mineral precipitation. Understanding the amount of CO_2 consumption when the groundwater and bedrock are at equilibrium can help us better predict possible shifts.

Using the average amount of CO_2 consumed per day, we calculated the partial pressure of CO_2 (PCO_2) in the soil. To do so, we found the Henry's Law constant for the average soil temperature during our recharge period (17.25 °C), in May, at our study site using the Kansas Mesonet website. This provided us with a Henry's Law constant of 2.74e-2 for that soil temperature. Using this constant, we estimated that the soil PCO_2 during the average recharge period is 0.2 atm (Fig. 8). This estimate is higher than expected, with another study on soil gases at the site measuring soil log pCO_2 to be between -2.1 and -1.1 (Tsypin and Macpherson, 2012), suggesting that CO_2 dissolution in water is not instantaneous. Instead, CO_2 is added over time as dissolved CO_2 in the groundwater is converted to alkalinity and more CO_2 can dissolve in its place (Kirk et al., 2013).

While carbonate weathering has the potential to take up more than half of the CO_2 present during recharge, some CO_2 is still expected to be released to the atmosphere once discharged into stream water (Fig. 8). Understanding CO_2 loss at the study site can provide insight into how outgassing may change depending on temperature and the amount of belowground mineral weathering taking place. To estimate loss, we used data from the two

stream sites (3-1 stream and 4-1 stream) and compared the CO_2 concentration at these sites with that of nearby wells (3-5 MOR and 4-6 MOR). These wells were chosen because their major chemistry was most similar to that of the stream water. Specifically, groundwater from these wells had sulfate, chloride, and fluoride concentrations that closely resembled the surface water concentrations. Based on differences in dissolved CO_2, we estimated that the average percent CO_2 loss from surface water outgassing was 5%, although that number could vary significantly with weather conditions and the solubility of CO_2. An average of 35% of the CO_2 initially present was retained in the stream water. Some portion of that 35% could be potentially lost downstream of the surface water sites focused on for this study.

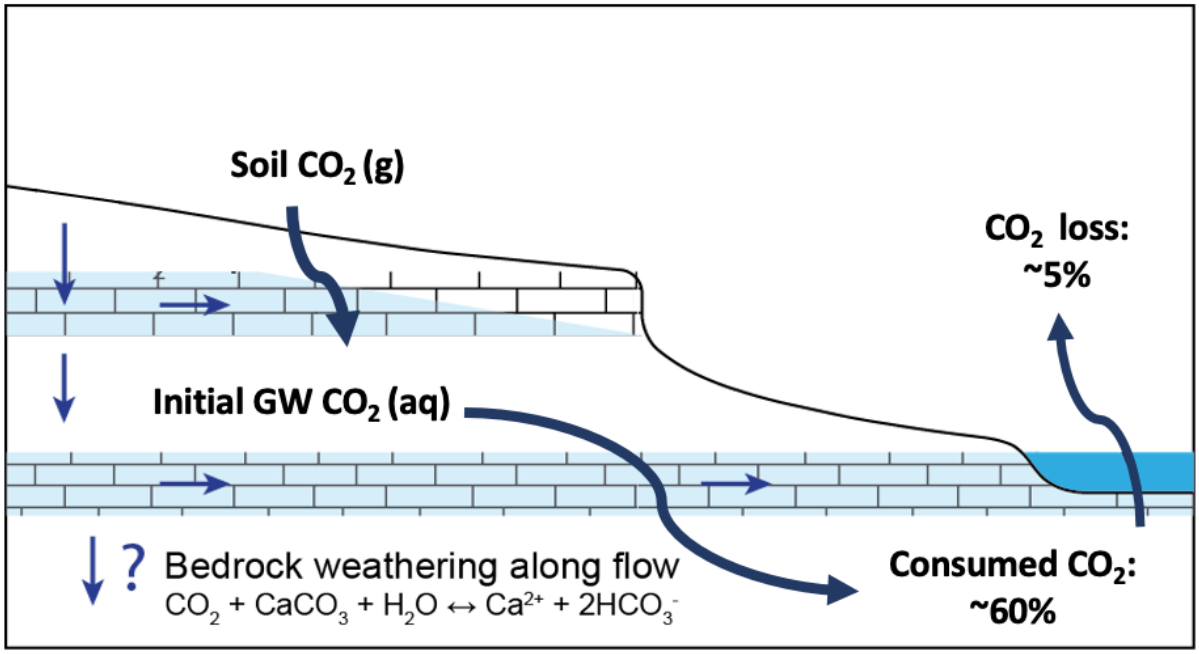

Figure 8. Soil CO_2 is carried to the groundwater during recharge, where it can be consumed by chemical weathering. CO_2 discharged at the stream has the potential to be lost to the atmosphere. Soil CO_2 partial pressure (PCO_2) was calculated by finding Henry's Law constant (2.74e-2) for the average May soil temperature (17.25 °C), which was found using the Kansas Mesonet website. This constant was then used to calculate PCO_2. We estimated that 60% of CO_2 is consumed through chemical weathering and that 5% is lost at the surface water.

4.4 Temporal Trends in Geochemistry

To better understand seasonal variation in watershed geochemistry, we compare our results to results collected previously by Macpherson and others (Macpherson et al., 2019). We focus our effort on data collected between 2014 and 2016. Prior to 2014, pH was measured in the lab rather than in the field. The pH of water samples is unstable and generally changes during storage (Macpherson, 2009). Therefore, by selecting 2014-2016 data, we decrease the likelihood that differences in pH between our dataset and the earlier data are from sample storage.

Seasonally, groundwater chemistry follows expected trends in root respiration and recharge (Fig. 9). Ca^{2+}, Mg^{2+}, and alkalinity vary similarly, with lowest values in the late winter to spring and highest values in late fall to winter. In contrast, pH, dissolved CO_2 concentrations, and the saturation indices of dolomite and calcite were lowest on average during spring and summer and highest during fall and winter.

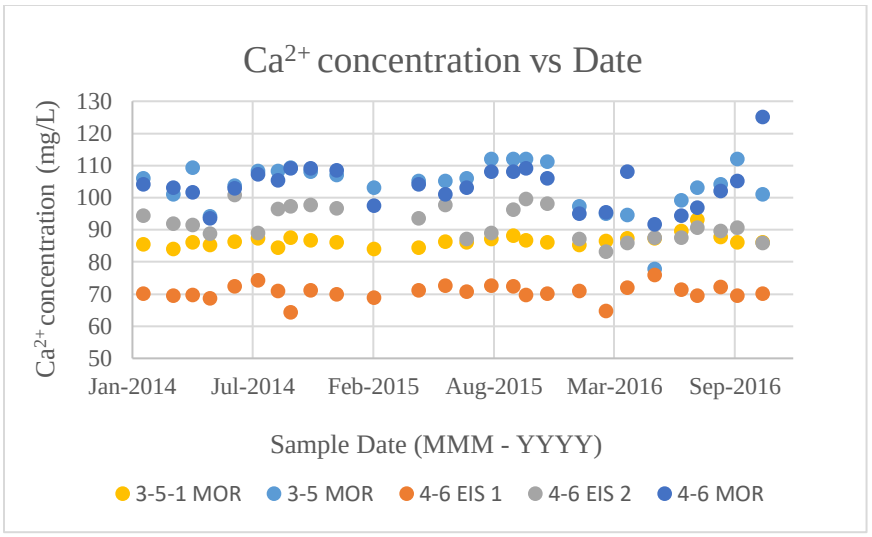
Ca2+ concentration vs Date
Ca2+ concentration (mg/L)
130
120
110
100
90
80
70
60
50
Jan-2014
Jul-2014
Feb-2015
Aug-2015
Mar-2016
Sep-2016
Sample Date (MMM - YYYY)
3-5-1 MOR
3-5 MOR
4-6 EIS 1
4-6 EIS 2
4-6 MOR

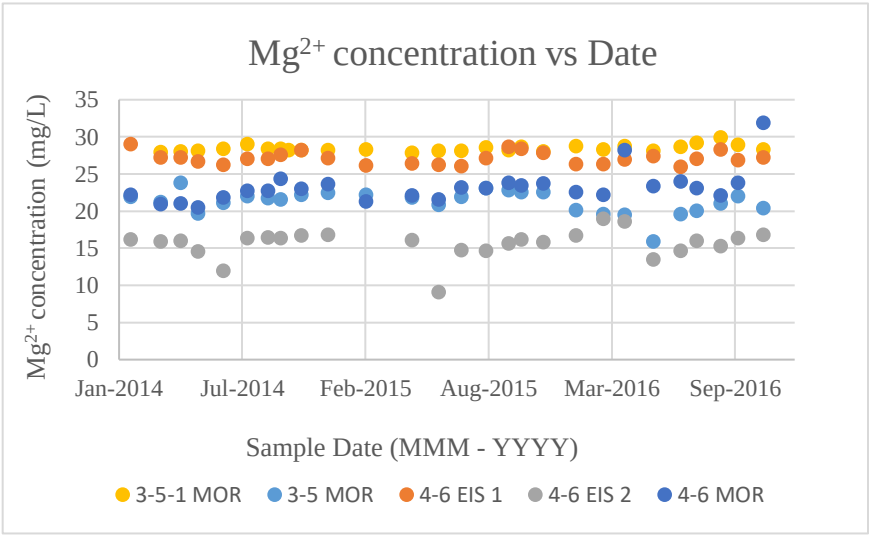
Mg2+ concentration vs Date
Mg2+ concentration (mg/L)
35
30
25
20
15
10
5
0
Jan-2014
Jul-2014
Feb-2015
Aug-2015
Mar-2016
Sep-2016
Sample Date (MMM - YYYY)
3-5-1 MOR
3-5 MOR
4-6 EIS 1
4-6 EIS 2
4-6 MOR

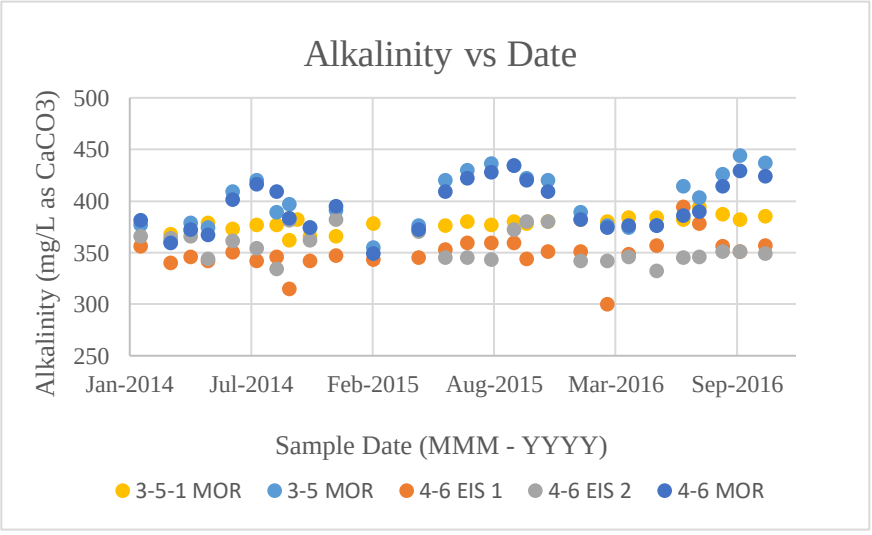
Alkalinity vs Date
Alkalinity (mg/L as CaCO3)
500
450
400
350
300
250
Jan-2014
Jul-2014
Feb-2015
Aug-2015
Mar-2016
Sep-2016
Sample Date (MMM - YYYY)
3-5-1 MOR
3-5 MOR
4-6 EIS 1
4-6 EIS 2
4-6 MOR

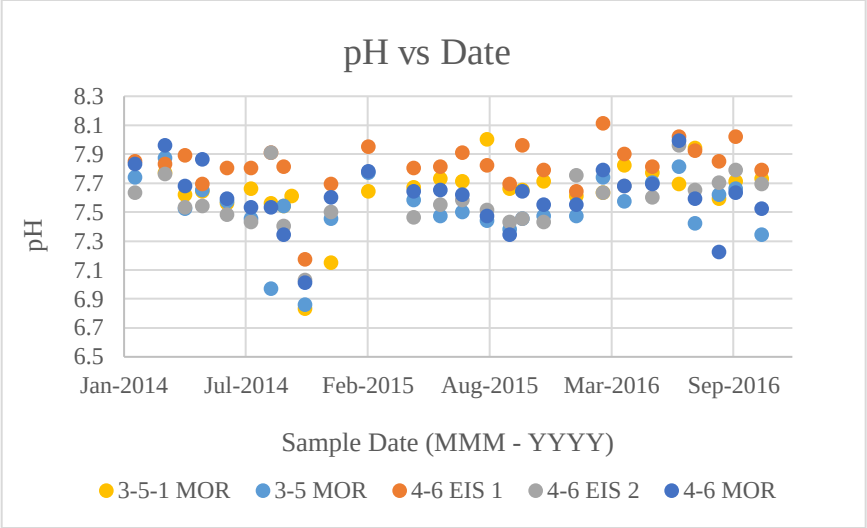
pH vs Date
pH
8.3
8.1
7.9
7.7
7.5
7.3
7.1
6.9
6.7
6.5
Jan-2014
Jul-2014
Feb-2015
Aug-2015
Mar-2016
Sep-2016
Sample Date (MMM - YYYY)
3-5-1 MOR
3-5 MOR
4-6 EIS 1
4-6 EIS 2
4-6 MOR

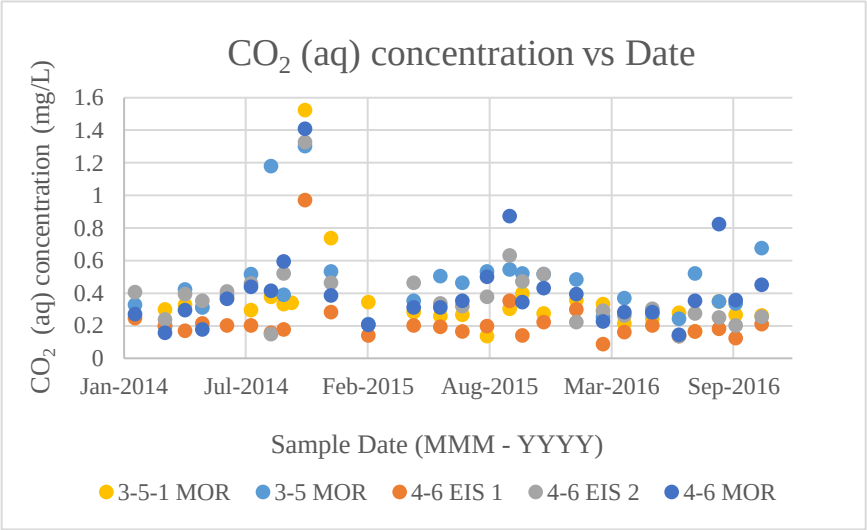
CO2 (aq) concentration vs Date
CO2 (aq) concentration (mg/L)
1.6
1.4
1.2
1
0.8
0.6
0.4
0.2
0
Jan-2014
Jul-2014
Feb-2015
Aug-2015
Mar-2016
Sep-2016
Sample Date (MMM - YYYY)
3-5-1 MOR
3-5 MOR
4-6 EIS 1
4-6 EIS 2
4-6 MOR

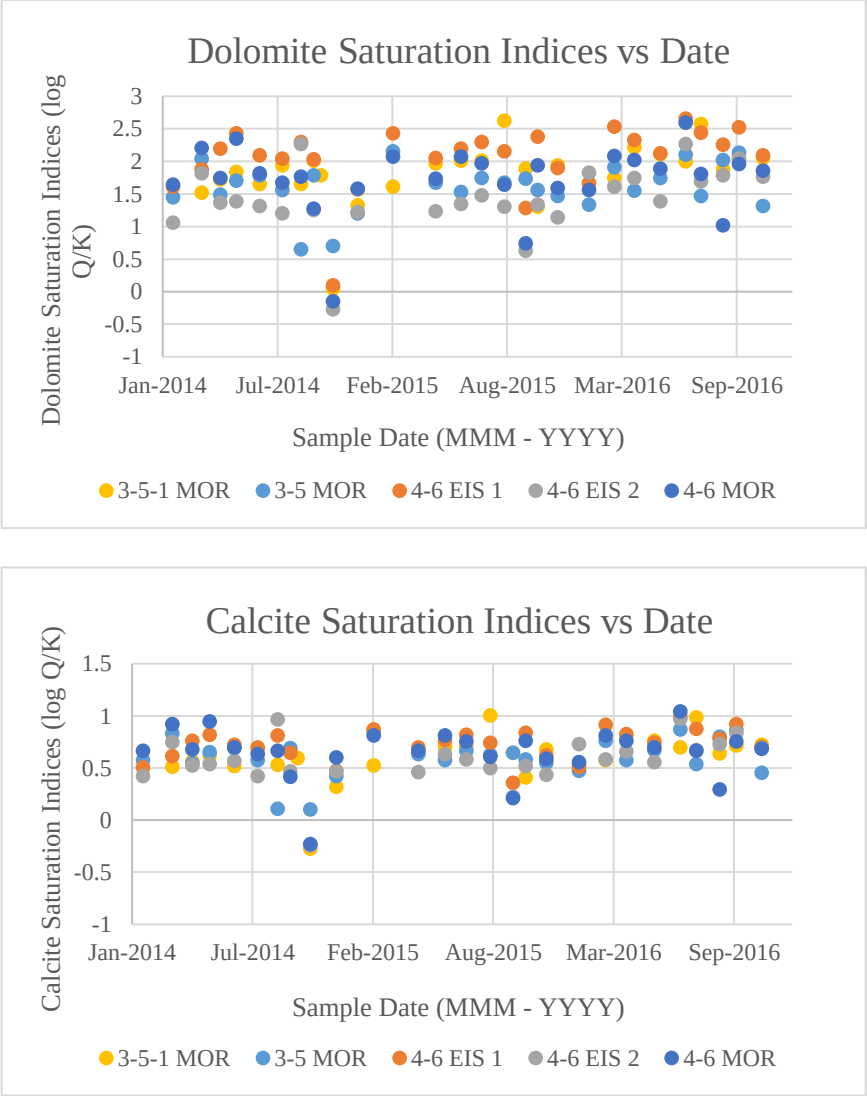

Figure 9. Ca^{2+} concentrations, Mg^{2+} concentrations, and alkalinity follow similar seasonal trends, with highest values in the late fall to winter and lowest in late winter to spring. The pH, CO_2 (aq) concentrations, and mineral saturation indices follow a different seasonal trend with lowest in spring and summer and highest values in fall and winter. Different colors correspond to different well sites (3-5-1 MOR, yellow; 3-5 MOR, light blue; 4-6 EIS 1, orange; 4-6 EIS 2, grey; 4-6 MOR, dark blue). Data is from Macpherson et al., 2019.

Applying the same methods and assumptions we used for our samples, we estimated that carbonate weathering consumed on average about 91% of the CO_2 that was initially present during recharge. On average, about 3.22 mmol CO_2 per liter of groundwater was consumed by carbonate weathering between 2014-2016.

These values are considerably greater than those estimated from our samples on average, which was 60% of CO_2 initially present. The difference appears to reflect the higher pH values measured for their samples (average pH = 7.28) compared to ours (average pH = 6.88). This difference could be the result of changing conditions. However, when we compare our results to the data from the same time frame in previous years, we still see that the previous data has higher pH values. Another possibility is that there were different sample handling and measurement methods between sampling teams. Other variables such as alkalinity and calcium and magnesium concentration were similar between both studies.

Despite differences between the previous dataset an our own, the previous dataset does provide insight into seasonal variation. Based on our calculations, CO_2 consumption was only slightly higher in the fall to early winter than spring and summer (Fig. 10). Overall, CO_2 consumption did not vary much from year to year, which is consistent with the groundwater being mostly in equilibrium with the bedrock.

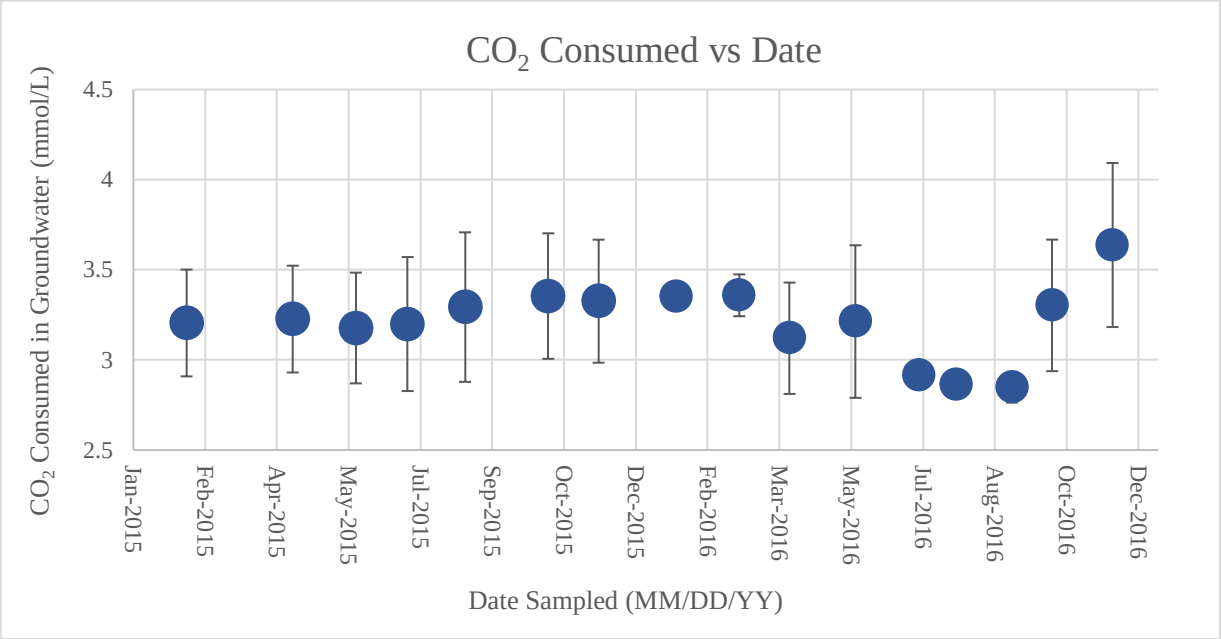

Figure 10. CO_2 consumed in groundwater plotted against the date sampled from 2015-2016, showing seasonal trends that reflect the chemical weathering of the bedrock. Each blue point represents averages for 5 well samples collected on same date and repeatedly sampled every 4-6 weeks. Error bars represent the standard deviation. Highest values fall between late fall to early winter and lowest are in the late spring to summer, reflecting trends in chemical weathering. Overall, there is not much variation in the data, suggesting that the groundwater is mostly in equilibrium with the bedrock. Data from Macpherson et al. (2019).

Lastly, we used the long-term data to compare trends in CO_2 outgassing with temperature. As surface water temperature increases, there is a statistically significant ($p < 0.05$) increase in CO_2 loss to the atmosphere (Fig. 11). These results coupled with the observed changes in stream calcite and dolomite saturation indices and dissolved CO_2 concentration with surface water temperature, demonstrate the temperature dependency of CO_2 outgassing in the watershed.

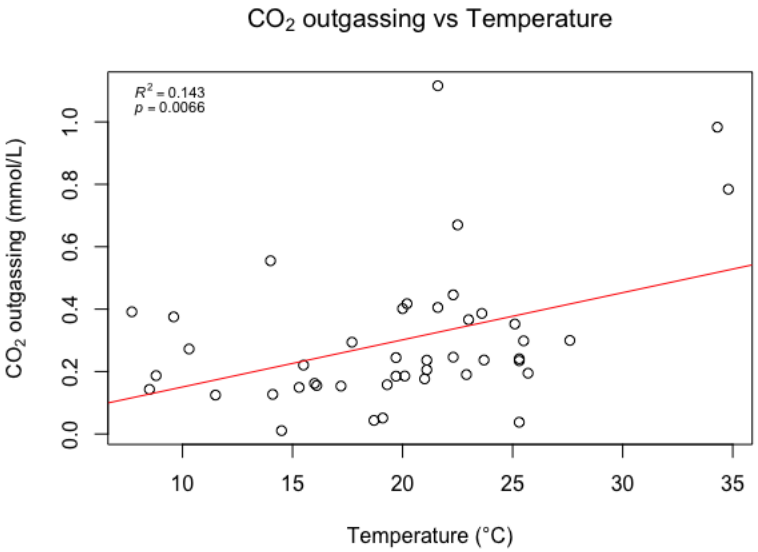

Figure 11. CO_2 outgassing plotted against temperature (°C), using data from 2014-2016 (Macpherson et al., 2019). The red line represents a best fit line. We observe a statistically significant ($p < 0.05$) increase in CO_2 outgassing with increased surface water temperature. However, the R^2 value is low due to other factors that influence CO_2 outgassing aside from temperature.

While these results are significant, the R^2 value is low, suggesting that temperature does not solely explain variations in CO_2 outgassing. Several other variables can contribute to CO_2 loss at the stream site, such as stream flow. Stream roughness and sinuous channel flow paths can cause surface water turbulence to be generated and effect gas exchange with the air. Increased discharge can also influence stream turbulence (Marx et al., 2017). Changes in solar radiation, which stimulates heterotopic metabolism, can affect CO_2 outgassing as well (Marx et al., 2017). Furthermore, the position in the stream can play a role in the observed amount of CO_2 loss. Rapid CO_2 outgassing is typical close recharge zones, where groundwater with a higher CO_2 concentration mixes with stream water (Marx et al., 2017).

Chapter 5 - Conclusions

Understanding the movement of CO_2 through a merokarst system can provide insight into the extent to which belowground carbonate weathering acts as a sink for CO_2 generated in soils. Isotopic data suggest that recharge took place predominantly around May, during months when the soil CO_2 is at its highest and could impact the amount of CO_2 present during recharge. Using atmospheric traces, we also estimated residence times within the aquifers to be relatively short. Our study reveals insignificant trends in solutes downgradient and with groundwater residence times. This, coupled with calcite saturation indices data, illustrates that the groundwater is generally in equilibrium with the carbonate bedrock, reflecting the rapid nature of carbonate weathering in karst environments. Our study also indicates that surface water is generally further from equilibrium with the carbonate bedrock than the groundwater. Additionally, the calcite saturation indices and dissolved CO_2 concentrations of the stream varies with water temperature. This demonstrates the temperature dependency of CO_2 outgassing.

Furthermore, our estimates for CO_2 consumption show the significance of carbonate weathering on CO_2 uptake (~60% dissolved CO_2 consumed during the study period). While estimates for CO_2 loss reveal that only a small percent of CO_2 is ultimately lost to the atmosphere when discharged at the stream. CO_2 loss was significantly impacted by the surface water temperature, emphasizing the importance of studying CO_2 movement through carbonate systems so we can better understand how it will be altered by Earth's changing climate. Overall, these results highlight that carbonate terrain, including merokarst, can play a significant role in CO_2 uptake and possibly have implications for the century-scale global CO_2 budget.

References

Barry, E.R., 2018, Characterizing groundwater flow through merokarst, Northeast Kansas, USA [Thesis]: University of Kansas.

Covington, M.D., Gulley, J.D., and Gabrovšek, F., 2015, Natural variations in calcite dissolution rates in streams: Controls, implications, and open questions: Geophysical Research Letters, v. 42, no. 8, p. 2836–2843.

Darling, W.G., Gooddy, D.C., MacDonald, A.M., and Morrris, B.L., 2012, The practicalities of using CFCs and SF6 for groundwater dating and tracing: Applied Geochemistry, v. 27, no. 9, p. 1688–1697.

Gaillardet, J., Calmels, D., Romero-Mujalli, G., Zakharova, E., and Hartmann, J., 2019, Global climate control on carbonate weathering intensity: Chemical Geology, v. 527, p. 118762.

Gaillardet, J., Dupré, B., Louvat, P., and Allègre, C.J., 1999, Global silicate weathering and CO2 consumption rates deduced from the chemistry of large rivers: Chemical Geology, v. 159, p. 3–30.

Gunal, H., and Ransom, M.D., 2005, Clay mineralogy, specific surface area and micromorphology of polygenetic soils from Eastern Kansas: Archives of Agronomy and Soil Science, v. 51, no. 4, p. 459–468.

Happell, J.D., Price, R.M., Top, Z., and Swart, P.K., 2003, Evidence for the removal of CFC-11, CFC-12, and CFC-113 at the groundwater–surface water interface in the Everglades: Journal of Hydrology, v. 279, no. 1, p. 94–105.

Hartmann, A., Goldscheider, N., Wagener, T., Lange, J., and Weiler, M., 2014, Karst water resources in a changing world: Review of hydrological modeling approaches: Reviews of Geophysics, v. 52, no. 3, p. 218–242.

Hendry, M.J., Mendoza, C.A., Kirkland, R.A., and Lawrence, J.R., 1999, Quantification of transient CO2 production in a sandy unsaturated zone: Water Resources Research, v. 35, no. 7, p. 2189–2198.

Kansas State University, Kansas Mesonet (n.d.). Manhattan, KS: Kansas State University. Retrieved from website at: https://mesonet.k-state.edu/agriculture/soiltemp/. Accessed 2021-03-22.

Kirk, M.F., Santillan, E.F.U., Sanford, R.A., and Altman, S.J., 2013, CO2-induced shift in microbial activity affects carbon trapping and water quality in anoxic bioreactors: Geochimica et Cosmochimica Acta, v. 122, p. 198–208.

Macpherson, G.L., 2009, CO2 distribution in groundwater and the impact of groundwater extraction on the global C cycle: Chemical Geology, v. 264, no. 1, p. 328–336.

Macpherson, G.L., 1996, Hydrogeology of thin limestones: the Konza Prairie Long-Term Ecological Research Site, Northeastern Kansas: Journal of Hydrology, v. 186, no. 1, p. 191–228.

Macpherson, G.L., Roberts, J.A., Blair, J.M., Townsend, M.A., Fowle, D.A., and Beisner, K.R., 2008, Increasing shallow groundwater CO2 and limestone weathering, Konza Prairie, USA: Geochimica et Cosmochimica Acta, v. 72, no. 23, p. 5581–5599.

Macpherson, G. 2019. AGW01 Long-term measurement of groundwater physical and chemical properties from wells on watershed N04D at Konza Prairie ver 12. Environmental Data Initiative. https://doi.org/10.6073/pasta/7e1ab16f473c2e3c03c6dad79b279db6. Accessed 2020-03-23.

Macpherson, G.L., and Sullivan, P.L., 2019, Watershed-scale chemical weathering in a merokarst terrain, northeastern Kansas, USA: Chemical Geology, v. 527, p. 118988.

Macpherson, G.L., Sullivan, P.L., Stotler, R.L., and Norwood, B.S., 2019, Increasing groundwater CO_2 in a mid-continent tallgrass prairie: Controlling factors (O. Chudaev, Y. Kharaka, R. Harmon, R. Millot, & O. Shouakar-Stash, Eds.): E3S Web of Conferences, v. 98, p. 06008.

Marx, A., Dusek, J., Jankovec, J., Sanda, M., Vogel, T., Geldern, R. van, Hartmann, J., and Barth, J. a. C., 2017, A review of CO2 and associated carbon dynamics in headwater streams: A global perspective: Reviews of Geophysics, v. 55, no. 2, p. 560–585.

Mason, J.A., and Jacobs, P.M., 1998, Chemical and particle-size evidence for addition of fine dust to soils of the midwestern United States: Geology, v. 26, p. 1135.

Mast, M.A., and Turk, J.T., 1999, Environmental Characteristics and Water Quality of Hydrologic Benchmark Network Stations in the Midwestern United States, 1963-95: U.S. Government Printing Office.

Nippert, J.B., and Knapp, A.K., 2007, Soil water partitioning contributes to species coexistence in tallgrass prairie: Oikos, v. 116, no. 6, p. 1017–1029.

Presley, D.R., Hartley, P.E., and Ransom, M.D., 2010, Mineralogy and morphological properties of buried polygenetic paleosols formed in late quaternary sediments on upland landscapes of the central plains, USA: Geoderma, v. 154, no. 3, p. 508–517.

Sánchez-Cañete, E.P., Barron-Gafford, G.A., and Chorover, J., 2018, A considerable fraction of soil-respired CO2 is not emitted directly to the atmosphere: Scientific Reports, v. 8, no. 1, p. 13518.

Simonson, R.W., 1995, Airborne dust and its significance to soils: Geoderma, v. 65, no. 1, p. 1–43.

Sullivan, P.L., Stops, M.W., Macpherson, G.L., Li, L., Hirmas, D.R., and Dodds, W.K., 2019, How landscape heterogeneity governs stream water concentration-discharge behavior in carbonate terrains (Konza Prairie, USA): Chemical Geology, v. 527, p. 118989.

The University of Utah, Online Isotopes in Precipitation Calculator (n.d.). Salt Lake City, Utah: The University of Utah. Retrieved from lab website at https://wateriso.utah.edu/waterisotopes/pages/data_access/form.html.

Tsypin, M., and Macpherson, G.L., 2012, The effect of precipitation events on inorganic carbon in soil and shallow groundwater, Konza Prairie LTER Site, NE Kansas, USA: Applied Geochemistry, v. 27, no. 12, p. 2356–2369.

Walker, S.J., Weiss, R.F., and Salameh, P.K., 2000, Reconstructed histories of the annual mean atmospheric mole fractions for the halocarbons CFC-11 CFC-12, CFC-113, and carbon tetrachloride: Journal of Geophysical Research: Oceans, v. 105, no. C6, p. 14285–14296.

Wen, H., Sullivan, P.L., Macpherson, G.L., Billings, S.A., and Li, L., 2021, Deepening roots can enhance carbonate weathering by amplifying CO_2-rich recharge: Biogeosciences, v. 18, no. 1, p. 55–75.

White, W.B., 2012, Conceptual Models for Carbonate Aquifers: Ground Water, v. 50, no. 2, p. 180–186.

Winnick, M.J., and Maher, K., 2018, Relationships between CO2, thermodynamic limits on silicate weathering, and the strength of the silicate weathering feedback: Earth and Planetary Science Letters, v. 485, p. 111–120.

Zeng, Z., and Tice, M.M., 2014, Promotion and nucleation of carbonate precipitation during microbial iron reduction: Geobiology, v. 12, no. 4, p. 362–371.

Appendix A - Geochemical Results

Table 1. Field measurement data for groundwater and surface water sites. Units for DO are mg/L, EC are mS/cm, T are °C, and alkalinity is meq/L

Well Name	Date	DO	pH	EC	T	Alk
1-1 stream	6/25/2020	n.a.	7.93	497.5	28.5	4.78
1-1 stream	8/6/2020	n.a.	7.18	520.5	20.5	4.92
3-1 stream	6/25/2020	n.a.	7.97	589.7	22.2	5.88
3-1 stream	8/6/2020	n.a.	7.07	611.4	18.8	6.26
3-1 stream	9/2/2020	8.4	7.9	630.9	21.4	6.51
3-1 stream	11/2/2020	n.a.	7.46	647.6	11.1	6.43
3-1 stream	12/1/2020	13.5	6.71	635	2.2	6.42
3-2MOR	9/21/2020	10	6.89	657.6	20.3	5.66
3-3 MOR	9/21/2020	8	7.13	683.2	19.5	3.99
3-3EIS	10/5/2020	7.7	7.07	567.7	20	5.5
3-5 MOR	6/25/2020	n.a.	7.04	488.7	19.4	6.2
3-5 MOR	8/6/2020	n.a.	6.65	655.3	16.7	6.77
3-5 MOR	9/2/2020	6.7	6.89	682.8	17.7	7.08
3-5 MOR	11/2/2020	7.4	6.8	773.6	17.4	6.94
3-5 MOR	12/1/2020	7.7	6.67	761.3	13.2	6.5
3-5-1 MOR	8/6/2020	n.a.	6.75	656.4	18.4	6.34
3-5-1 MOR	10/12/2020	1.9	6.89	649.9	13.3	6.18
3-5-1MOR	9/21/2020	7.3	7.14	n.a.	15.9	6.53
3-5-1MOR	11/2/2020	1.7	6.94	649.4	16.2	6.27
3-5-1MOR	12/1/2020	2.3	6.65	596.6	12.7	6.21
4-1 stream	6/25/2020	n.a.	7.46	596.7	17.4	6.21
4-1 stream	8/6/2020	n.a.	18.1	644.6	18.1	6.7
4-1Stream	9/4/2020	8.3	7.19	667.7	22.7	6.83
4-1Stream	11/2/2020	10.4	6.61	660.7	9.4	6.72
4-1Stream	12/1/2020	9.1	6.65	631.5	6	6.59

Well Name	Date	DO	pH	EC	T	Alk
4-2EIS1	9/4/2020	5.8	6.93	732.3	26.8	7.08
4-2EIS1	10/12/2020	1.4	6.89	858.4	17.8	7.13
4-2EIS1	10/19/2020	2.1	6.73	855.7	12.8	7.04
4-2EIS2	9/4/2020	4.1	6.9	736.3	17.7	6.78
4-2EIS2	10/5/2020	3.4	6.73	718.2	18	6.68
4-6 EIS 1	8/6/2020	n.a.	6.72	581.8	16	5.77
4-6 EIS 2	8/6/2020	n.a.	6.89	566.8	17.8	7.57
4-6 MOR	6/25/2020	n.a.	7.19	459.2	20.2	6.01
4-6 MOR	8/6/2020	n.a.	6.8	625.5	16.9	6.63
4-6 MOR	9/14/2020	5.6	6.84	706.5	18	6.88
4-6EIS1	9/14/2020	n.a.	6.95	747.5	17.7	6.72
4-6EIS1	11/2/2020	n.a.	6.99	736.5	14.2	5.85
4-6EIS1	12/1/2020	7.6	6.78	556.2	12.1	5.77
4-6EIS2	9/1/2020	9.2	6.93	557.3	19.8	5.97
4-6EIS2	9/14/2020	7.1	6.81	726.3	16.5	8.31
4-6EIS2	11/2/2020	6.9	6.78	642.3	15.6	6.79
4-6EIS2	12/1/2020	5.8	6.72	671.3	13.4	6.59
4-6MOR	9/1/2020	8.3	6.81	652.4	15.8	6.98
4-6MOR	9/14/2020	6.5	7.03	686.2	15.4	6.91
4-6MOR	11/2/2020	n.a.	6.77	987.9	15.3	6.99
4-6MOR	12/1/2020	7.7	6.84	661.4	13	6.46

Table 2. Major anion data for groundwater and surface water. Units are mg/L for all parameters.

Well Name	Date	F^-	Cl^-	Br^-	NO_3^-	SO_4^{2}
1-1 stream	6/25/2020	0.3854	2.5727	n.a.	0.1344	23.7094
1-1 stream	8/6/2020	0.3733	2.6035	n.a.	0.2997	35.7207
3-1 stream	6/25/2020	0.3948	2.4632	n.a.	0.1492	23.5491
3-1 stream	8/6/2020	0.3933	2.7928	n.a.	0.3025	35.6575
3-1 stream	9/2/2020	0.3531	2.7386	n.a.	0.6044	41.3639
3-1 stream	11/2/2020	0.3921	2.7613	n.a.	0.0562	48.535
3-1 stream	12/1/2020	0.4292	3.3028	n.a.	0.5677	57.1602
3-2MOR	9/21/2020	0.3594	2.326	n.a.	0.5206	14.2509
3-3 MOR	9/21/2020	1.2567	26.6382	0.0204	1.3611	54.4327
3-3EIS	10/5/2020	0.3366	2.1092	n.a.	0.4422	7.8221
3-5 MOR	6/25/2020	0.4652	3.3339	n.a.	0.2728	17.3919
3-5 MOR	8/6/2020	0.4678	3.2465	0.0113	0.2803	23.4367
3-5 MOR	9/2/2020	0.4184	2.4502	3.5625	0.7422	30.1834
3-5 MOR	11/2/2020	0.3831	2.8843	n.a.	0.1388	38.2324
3-5 MOR	12/1/2020	0.4197	3.1654	n.a.	0.1155	44.152
3-5-1 MOR	8/6/2020	0.3546	4.0757	n.a.	0.3437	42.6005
3-5-1 MOR	10/12/2020	0.403	3.8832	0.0541	0.1721	43.59
3-5-1MOR	9/21/2020	0.4058	3.6757	0.0092	0.4251	42.3469
3-5-1MOR	11/2/2020	0.3544	3.4324	n.a.	0.1387	39.891
3-5-1MOR	12/1/2020	0.3921	3.6999	n.a.	0.2359	40.1122
4-1 stream	6/25/2020	0.4037	2.4223	0.0064	0.1376	17.7866
4-1 stream	8/6/2020	0.3858	2.4718	0.0038	0.2932	27.2427
4-1Stream	9/4/2020	0.3906	2.4754	2.3279	0.7765	38.2667
4-1Stream	11/2/2020	0.3667	2.7205	n.a.	0.1367	45.559
4-1Stream	12/1/2020	0.3725	3.1363	n.a.	0.4596	51.1716
4-2EIS1	9/4/2020	0.3857	6.2016	0.0216	0.8313	35.0482
4-2EIS1	10/12/2020	0.4169	3.1068	0.0503	0.4011	34.706
4-2EIS1	10/19/2020	0.4427	3.2531	0.0497	0.3682	36.2047

Well Name	Date	F^-	Cl^-	Br^-	NO_3^-	SO_4^{2}
4-2EIS2	9/4/2020	0.3992	2.4741	0.0451	0.8507	38.0458
4-2EIS2	10/5/2020	0.4264	2.8954	0.031	0.4755	31.4557
4-6 EIS 1	8/6/2020	0.4228	3.2281	n.a.	1.0684	18.8082
4-6 EIS 2	8/6/2020	0.423	4.9192	n.a.	0.677	13.9518
4-6 MOR	6/25/2020	0.426	3.7328	n.a.	0.9795	23.1355
4-6 MOR	8/6/2020	0.4198	3.2743	0.0076	0.4348	26.8286
4-6 MOR	9/14/2020	0.4026	2.4626	1.5612	0.3922	32.2183
4-6EIS1	9/14/2020	0.4254	2.846	n.a.	1.4848	21.9159
4-6EIS1	11/2/2020	0.4727	3.1594	0.0067	0.9151	20.3496
4-6EIS1	12/1/2020	0.4698	3.058	n.a.	1.0479	21.8192
4-6EIS2	9/1/2020	0.3575	2.3909	2.0247	0.807	12.178
4-6EIS2	9/14/2020	0.3847	2.3466	0.0157	0.7295	10.9863
4-6EIS2	11/2/2020	0.3443	2.3525	n.a.	0.3174	10.0979
4-6EIS2	12/1/2020	0.4008	2.7842	0.0357	0.3313	11.6542
4-6MOR	9/1/2020	0.4166	2.5019	0.0248	0.8354	28.885
4-6MOR	9/14/2020	0.4039	2.826	1.3203	0.4834	34.5257
4-6MOR	11/2/2020	0.3722	60.5955	0.0121	0.3519	38.2842
4-6MOR	12/1/2020	0.3956	3.3288	n.a.	0.2509	44.4666

Table 3. Major cation data for groundwater and surface water samples. Units are mg/L for all parameters.

Well Name	Date	Na^+	K^+	Mg^{2+}	Ca^{2+}	Sr^{2+}
1-1 stream	6/25/2020	3.8857	0.9339	18.0962	86.058	3.1
1-1 stream	8/6/2020	4.5651	1.0174	18.9471	68.1245	3.538
3-1 stream	6/25/2020	3.8301	0.9779	18.5324	86.058	4.1484
3-1 stream	8/6/2020	4.2576	0.9083	17.7648	94.205	3.9548
3-1 stream	9/2/2020	5.0078	1.5202	21.987	64.474	4.5675
3-1 stream	11/2/2020	5.0096	1.5057	21.904	106.201	4.6225
3-1 stream	12/1/2020	5.2797	0.6374	20.853	100.614	4.6835
3-2MOR	9/21/2020	2.7321	0.9674	13.032	90.658	3.8262
3-3 MOR	9/21/2020	16.4688	35.602	38.519	40.582	6.2047
3-3EIS	10/5/2020	2.3367	0.7445	8.6896	83.967	3.7601
3-5 MOR	6/25/2020	4.7788	2.3752	21.1019	98.067	4.2312
3-5 MOR	8/6/2020	5.1179	2.0703	19.8893	99.272	4.4133
3-5 MOR	9/2/2020	4.1364	1.043	19.3495	100.382	4.0605
3-5 MOR	11/2/2020	4.7887	1.037	20.6244	110.646	4.7644
3-5 MOR	12/1/2020	5.3016	1.0482	20.1045	117.324	4.8978
3-5-1 MOR	8/6/2020	6.8096	1.6998	28.5385	86.7915	5.0864
3-5-1 MOR	10/12/2020	6.7182	1.312	32.587	104.707	5.2744
3-5-1MOR	9/21/2020	6.5058	1.9272	33.575	89.873	4.9067
3-5-1MOR	11/2/2020	6.5183	1.3531	27.273	84.061	4.9477
3-5-1MOR	12/1/2020	7.1529	1.1248	27.779	86.984	5.0359
4-1 stream	6/25/2020	3.6878	0.8427	18.3408	113.203	4.0865
4-1 stream	8/6/2020	4.4235	0.9269	18.8963	105.968	4.3124
4-1Stream	9/4/2020	5.0068	1.4428	21.586	109.378	5.0797
4-1Stream	11/2/2020	4.9244	1.0182	21.464	107.192	4.5671
4-1Stream	12/1/2020	5.0746	0.3135	20.7871	107.118	4.5257
4-2EIS1	9/4/2020	5.7663	6.1942	24.004	104.295	5.7807
4-2EIS1	10/12/2020	5.2318	1.3237	25.052	105.489	5.9027

Well Name	Date	Na^{+}	K^{+}	Mg^{2+}	Ca^{2+}	Sr^{2+}
4-2EIS1	10/19/2020	5.122	1.4	24.312	103.529	5.7843
4-2EIS2	9/4/2020	4.7141	1.2902	19.4123	89.607	4.4533
4-2EIS2	10/5/2020	4.8674	1.265	18.5243	99.858	4.3473
4-6 EIS 1	8/6/2020	6.8698	2.0175	24.6165	76.689	4.5019
4-6 EIS 2	8/6/2020	4.6865	3.4379	15.1032	105.65	3.9155
4-6 MOR	6/25/2020	4.3869	2.5066	19.1984	109.743	4.0013
4-6 MOR	8/6/2020	5.0142	1.812	22.275	99.581	4.4501
4-6 MOR	9/14/2020	4.7321	1.2058	20.021	99.279	4.8673
4-6EIS1	9/14/2020	6.7604	2.4027	25.509	77.2225	4.1456
4-6EIS1	11/2/2020	6.8711	1.9678	24.505	75.272	4.2346
4-6EIS1	12/1/2020	7.2166	1.0675	26.0305	76.0055	4.2752
4-6EIS2	9/1/2020	2.9027	0.6223	14.9176	87.796	3.3344
4-6EIS2	9/14/2020	3.4552	1.2337	15.814	90.022	3.6374
4-6EIS2	11/2/2020	3.8044	0.7195	16.2258	99.072	3.7485
4-6EIS2	12/1/2020	6.7038	0.472	15.3123	97.078	3.7223
4-6MOR	9/1/2020	4.4166	1.1061	20.3561	95.245	4.5129
4-6MOR	9/14/2020	4.9162	1.1572	26.872	125.496	4.6534
4-6MOR	11/2/2020	12.7158	58.633	21.672	100.503	4.8403
4-6MOR	12/1/2020	5.4193	0.7632	17.754	80.946	4.7159

Table 4. Dissolved CO_2 concentrations and calcite and dolomite saturation indices (SI) for groundwater and surface water samples. Units for CO_2 (aq) are free mmol and units for the saturation indices are log Q/K.

Well Name	Date	CO_2 (aq)	Calcite SI	Dolomite SI
1-1 stream	6/25/2020	0.1149	1.028	2.541
1-1 stream	8/6/2020	0.7399	0.09165	0.7402
3-1 stream	6/25/2020	0.137	1.059	2.579
3-1 stream	8/6/2020	1.226	0.1819	0.7437
3-1 stream	9/2/2020	0.1817	0.8933	2.444
3-1 stream	11/2/2020	0.5651	0.51	1.392
3-1 stream	12/1/2020	3.762	-0.385	-0.4562
3-2MOR	9/21/2020	1.661	-0.01704	0.2347
3-3 MOR	9/21/2020	0.6798	-0.3014	0.4814
3-3EIS	10/5/2020	1.074	0.1237	0.3708
3-5 MOR	6/25/2020	1.288	0.177	0.7941
3-5 MOR	8/6/2020	3.594	-0.2109	-0.02844
3-5 MOR	9/2/2020	2.125	0.06063	0.505
3-5 MOR	11/2/2020	2.565	-0.006198	0.3553
3-5 MOR	12/1/2020	3.468	-0.1953	-0.08643
3-5-1 MOR	8/6/2020	2.608	-0.18	0.2597
3-5-1 MOR	10/12/2020	1.958	-0.05094	0.4618
3-5-1MOR	9/21/2020	1.121	0.1944	1.049
3-5-1MOR	11/2/2020	1.714	-0.03735	0.525
3-5-1MOR	12/1/2020	3.49	-0.3651	-0.1598
4-1 stream	6/25/2020	0.4975	0.6232	1.552
4-1 stream	8/6/2020	4.70E-18	1.541	1.201
4-1Stream	9/4/2020	0.9576	0.4421	1.31
4-1Stream	11/2/2020	4.349	-0.3352	-0.3234
4-1Stream	12/1/2020	4.126	-0.353	-0.3949
4-2EIS1	9/4/2020	1.737	0.2352	0.9874

Well Name	Date	CO_2 (aq)	Calcite SI	Dolomite SI
4-2EIS1	10/12/2020	2.124	0.07824	0.632
4-2EIS1	10/19/2020	3.265	-0.1631	0.1126
4-2EIS2	9/4/2020	1.996	0.005976	0.4462
4-2EIS2	10/5/2020	2.897	-0.1183	0.1315
4-6 EIS 1	8/6/2020	2.647	-0.3173	-0.04299
4-6 EIS 2	8/6/2020	2.27	0.1166	0.4875
4-6 MOR	6/25/2020	0.8704	0.3671	1.09
4-6 MOR	8/6/2020	2.476	-0.06873	0.3049
4-6 MOR	9/14/2020	2.31	-0.001935	0.4012
4-6EIS1	9/14/2020	1.766	-0.005092	0.6064
4-6EIS1	11/2/2020	1.474	-0.07738	0.4316
4-6EIS1	12/1/2020	2.44	-0.3175	-0.04023
4-6EIS2	9/1/2020	1.606	0.02335	0.3856
4-6EIS2	9/14/2020	3.064	-0.00806	0.3202
4-6EIS2	11/2/2020	2.716	-0.08827	0.1216
4-6EIS2	12/1/2020	3.127	-0.1989	-0.1307
4-6MOR	9/1/2020	2.59	-0.07185	0.2726
4-6MOR	9/14/2020	1.527	0.2385	0.8925
4-6MOR	11/2/2020	2.837	-0.1169	0.1863
4-6MOR	12/1/2020	2.345	-0.1799	0.0494

Appendix B - Hydrology Data

Table 5. Depth to water (DTW), total depth (TD), and measuring point (MP) evaluation data are in units of meters. Depth to water was measured before sampling the well.

Well Name	Date	DTW	TD	MP Elevation
1-6MOR	9/21/2020	7.900416	8.24484	372.184
2-6 MOR	9/21/2020	7.866888	8.19912	372.323
3-2MOR	9/21/2020	7.86384	8.21436	372.322
3-3 MOR	9/21/2020	11.29284	11.75004	375.801
3-3EIS	9/8/2020	4.47294	6.477	375.756
3-3EIS	10/5/2020	4.392168	6.46176	375.756
3-5 MOR	6/25/2020	6.27888	6.82752	370.588
3-5 MOR	8/6/2020	6.33984	6.82752	370.588
3-5 MOR	9/2/2020	6.342888	6.84276	370.588
3-5 MOR	11/2/2020	6.132576	6.84276	370.588
3-5 MOR	12/1/2020	6.37032	6.84276	370.588
3-5-1 MOR	8/6/2020	10.69848	12.67968	374.803
3-5-1 MOR	10/12/2020	10.948416	12.573	374.803
3-5-1MOR	9/21/2020	10.92708	12.60348	374.803
3-5-1MOR	11/2/2020	10.92708	12.55776	374.803
3-5-1MOR	12/1/2020	10.869168	12.573	374.803
3-6MOR	9/21/2020	4.919472	5.184648	374.164
3-7EIS	9/1/2020	22.26564	22.87524	393.389
4-2 MOR	6/25/2020	10.94232	11.06424	374.651
4-2 MOR	8/6/2020	10.94232	11.06424	374.651
4-2 MOR	11/2/2020	10.945368	11.06424	374.651
4-2 MOR	12/1/2020	10.94232	11.06424	374.651
4-2EIS1	9/4/2020	3.5052	5.873496	374.6
4-2EIS1	10/12/2020	3.70332	5.876544	374.6
4-2EIS1	10/19/2020	3.7338	5.876544	374.6

Well Name	Date	DTW	TD	MP Elevation
4-2EIS2	9/4/2020	3.71856	4.52628	374.507
4-2EIS2	10/5/2020	3.71856	4.51104	374.507
4-6 EIS 1	6/25/2020	6.7056	7.58952	375.783
4-6 EIS 1	8/6/2020	6.76656	7.86384	375.783
4-6 EIS1	9/1/2020	6.793992	7.58952	375.783
4-6 EIS1	9/14/2020	6.84276	7.57428	375.783
4-6 EIS1	11/2/2020	6.82752	7.62	375.783
4-6 EIS1	12/1/2020	6.81228	7.58952	375.783
4-6 EIS2	6/25/2020	4.953	5.65404	375.795
4-6 EIS2	8/6/2020	5.66928	5.0292	375.795
4-6 EIS2	9/1/2020	5.0292	5.644896	375.795
4-6 EIS2	9/14/2020	5.04444	5.6388	375.795
4-6 EIS2	11/2/2020	5.04444	5.66928	375.795
4-6 EIS2	12/1/2020	4.425696	5.035296	375.795
4-6 MOR	6/25/2020	11.76528	12.74064	375.816
4-6 MOR	8/6/2020	12.00912	12.74064	375.816
4-6 MOR	9/14/2020	12.07008	12.722352	375.816
4-6 MOR	9/1/2020	12.0396	12.7254	375.816
4-6 MOR	9/14/2020	12.07008	12.722352	375.816
4-6 MOR	11/2/2020	12.08532	12.7254	375.816
4-6 MOR	12/1/2020	12.02436	12.4206	375.816

Appendix C - NPOC and Isotope Data

Table 6. Non-purgeable organic carbon (NPOC), dissolved inorganic carbon (DIC) $\delta^{13}C$**,** water isotope data for groundwater and surface water. NPOC values are in units of mg/L, $\delta^{13}C$-DIC is reported in per mil VPDB. Oxygen ($\delta^{18}O$) and hydrogen (δD) isotopic values are reported in parts per mil VSMOW. E stands for estimated value because the concentration exceeded the level of high standard. An asterisk (*) symbolizes the sample was collected with a pump, all other samples were collected with a bailer.

Well Name	Date	NPOC	$\delta^{13}C$-DIC	$\delta^{18}O$ (H_2O)	δD (H_2O)
3-2MOR	9/21/2020	3.195	-7.28	-4.2	-28
3-3 MOR	9/21/2020	1.87	-5.07	-4.2	-31
3-3EIS	10/5/2020	0.9073	-5.53	-4	-28
3-5 MOR*	9/2/2020	0.8678	-9.95	-4.2	-27
3-5 MOR	11/2/2020	4.376	-9.83	n/a	n/a
3-5-1 MOR	10/12/2020	E7.433	-6.48	-4.1	-29
3-5-1MOR	9/21/2020	E20.39	-6.79	-4.5	-29
4-2EIS1*	9/4/2020	1.286	-7.41	-4.4	-28
4-2EIS1	10/12/2020	1.492	-7.61	-4.3	-29
4-2EIS1	10/19/2020	3.176	-7.54	-4.5	-29
4-2EIS2	9/4/2020	2.225	-7.77	-4.2	-28
4-2EIS2	10/5/2020	2.424	-7.86	-3.9	-28
4-6 EIS1	9/14/2020	1.524	-6.62	-4.3	-29
4-6 EIS2*	9/1/2020	0.7048	-6.73	-4	-28
4-6 EIS2	9/14/2020	2.965	-4.72	-4	-28
4-6 MOR	9/14/2020	1.372	-10.00	-3.8	-28
4-6 MOR*	9/14/2020	0.8637	-10.04	-4.3	-28
4-6 MOR*	9/1/2020	0.8839	-9.57	-4.2	-27
3-1 Stream	9/2/20	n/a	-6.79	-4.1	-27
4-1 Stream	9/4/20	n/a	-10.04	-4.1	-27

Appendix D - Atmospheric Tracer Results

Table 7. Atmospheric tracer data, including concentrations of chlorofluorocarbons (CFC-12, CFC-11, CFC-113) and sulfur hexafluoride (SF_6), for groundwater in both the Morrill and Eiss Limestone aquifers. All tracers are in units of years. Three replicates were taken for each sample, the table below lists the averages of these three replicates except for 3-5-1 MOR, for which two replicate samples were broken in transport. An asterisk (*) symbolizes the sample was collected with a pump, all other samples were collected with a bailer.

Well Name	Date	CFC 12	CFC 11	CFC 113	SF_6
4-6 MOR*	9/1/20	36.67	44.00	33.67	13.67
4-6 EIS2*	9/1/20	33.67	39.00	33.00	22.00
3-5 MOR*	9/2/20	37.00	43.00	34.00	22.50
4-6 MOR	9/14/20	39.67	44.33	35.33	18.67
4-6 MOR*	9/14/20	37.67	43.00	34.67	12.00
4-2 EIS1	10/19/20	35.33	43.00	33.00	2.33
4-2 EIS2	10/5/20	34.00	41.33	32.00	4.00
4-2 EIS2	10/5/20	34.33	42.00	33.00	4.33
3-3 EIS	10/5/20	38.00	42.33	34.33	5.00
3-5-1 MOR	10/12/20	49.00	53.00	43.00	35.00

Appendix E - Detection Limits and Precision

Table 8. Detections limits and precision for the Ion Chromatograph (IC). Units are in mg/L.

CS-1100 Ion Chromatograph (IC)	F^-	Cl^-	Br^-	NO_3^-	SO_4^{2}	Na^+	K^+	Mg^{2+}	Ca^{2+}	Sr^{2+}
MDL	0.08	0.68	0.058	0.59	0.81	1.51	0.44	0.40	0.41	0.53
Precision	0.05	0.43	0.04	0.38	0.52	1.01	0.16	0.27	0.27	0.35

Appendix F - CO_2 calculations

We performed CO_2 calculations to determine the amount of CO_2 consumed, lost, and initially present using observed concentrations of Ca^{2+} and Mg^{2+} as well as calculated dissolved CO_2 concentrations. We began by determining the amount of CO_2 consumed during dolomite dissolution. Given the chemical equation for dolomite weathering, we used the follow equation:

$$\text{mM } (CaMg)(CO_3)_2 * \frac{2 \text{ mM } CO_2}{1 \text{ mM } (CaMg)(CO_3)_2} = \text{mM } CO_2 \text{ consumed by dolomite dissolution}$$

We then subtracted the Ca^{2+} concentrations from the Mg^{2+} concentration to give us the Ca^{2+} concentrations remaining after dolomite dissolution. This concentration was used to determine CO_2 consumed during calcite weathering. Given the chemical equation for calcite dissolution, we used the follow equation:

$$\text{mM } (CaCO_3) * \frac{1\text{mM } CO_2}{1 \text{ mM } (CaCO_3)} = \text{mM } CO_2 \text{ consumed by calcite dissolution}$$

We then combined the values for CO_2 consumed during calcite and dolomite dissolution to get the total CO_2 consumed within the groundwater by carbonate weathering, assuming all calcium and magnesium present in the groundwater is derived from carbonate mineral weathering. To determine the initial CO_2 content of the groundwater, we added the calculated CO_2 value to the CO_2 values we observed, or CO_2 present. To determine CO_2 loss, we subtracted the present dissolved CO_2 concentrations in the surface water from the present dissolved CO_2 concentrations in a nearby well with similar chemistry.